Generalised curvilinear coordinates, vertical discretisations, and moving mesh adaptivity in atmospheric numerical models

Christian Kühnlein

ECMWF

Main topics of the lecture (2h)

Main topics of this lecture:

1. Governing PDEs of atmospheric dynamics in generalised curvilinear coordinates
2. Vertical coordinates/discretisation in some atmospheric models
3. Adaptive (moving) meshes

Generalised curvilinear coordinate mappings

- ...transform governing PDEs to more convenient coordinates for solution
- ...accommodate complex boundaries
- ...apply a variable-resolution mesh
- ...apply dynamic mesh adaptivity

General curvilinear coordinate mappings

$$(\overline{x}, \overline{y}) = (E(x, y), D(x, y)) : \quad \mathcal{D}_p \to \mathcal{D}_t$$

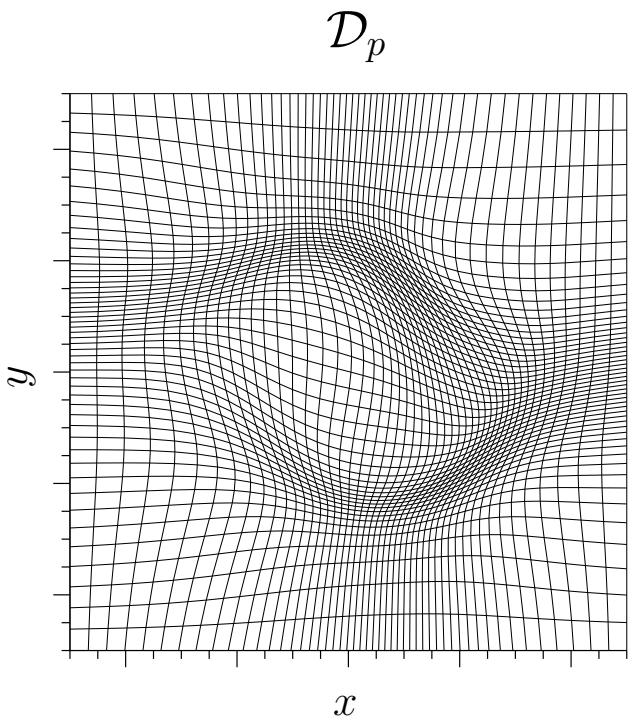

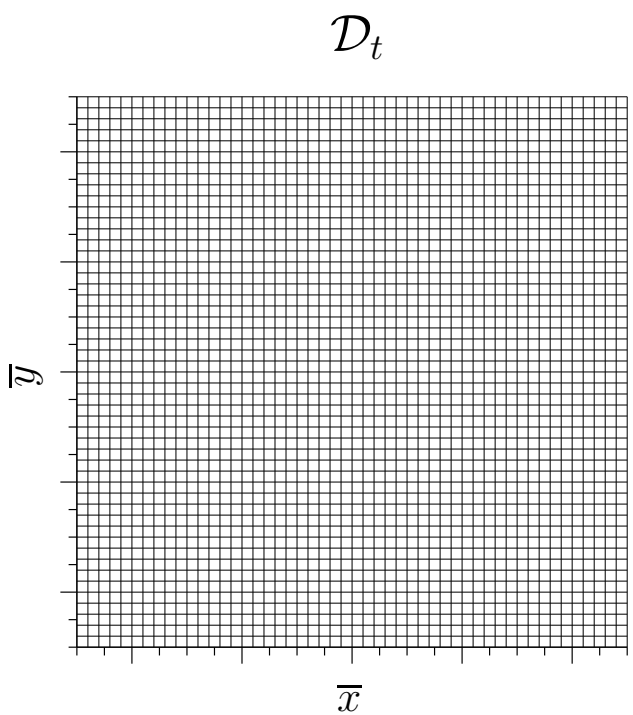

General curvilinear coordinate mappings

General bijective coordinate mapping:

$$(\overline{t}, \overline{\mathbf{x}}) = (t, \mathcal{F}(t, \mathbf{x})) : \quad \mathcal{D}_p \rightarrow \mathcal{D}_t$$

- $\mathcal{D}_p$ is subdomain of the physical space $\mathbf{S}_p$ – with coordinates $(t, \mathbf{x}) \equiv (t, x, y, z)$ and metric tensor g_{kj} – where the physical problem is posed. It is convenient to assume the physical system $\mathbf{S}_p$ to be a stationary and orthogonal (e.g. Cartesian, geospherical, spheroidal,..)
- $\mathcal{D}_t$ is subdomain of transformed computational space $\mathbf{S}_t$ – with generalised coordinates $(\overline{t}, \overline{\mathbf{x}}) \equiv (\overline{t}, \overline{x}, \overline{y}, \overline{z})$ and metric tensor $\overline{g}_{rs}$ – where the problem is solved

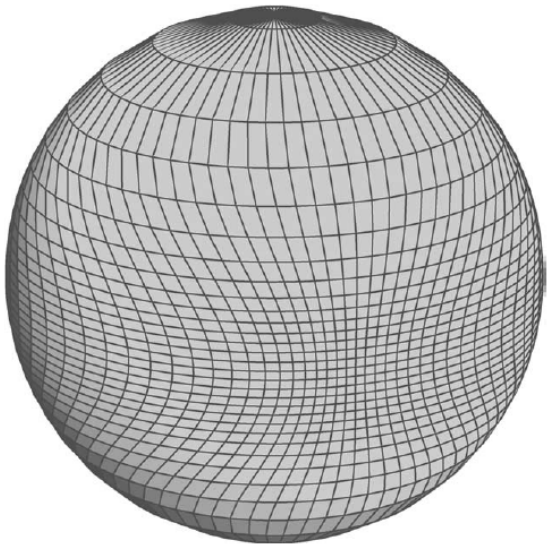

Governing equations in Lagrangian form

Symbolic vector-form of basic adiabatic governing PDEs:

$$\frac{D\mathbf{u}}{Dt} = -c_p\theta\nabla\pi + \mathbf{g} + \mathbf{M}$$

$$\frac{D\theta}{Dt} = 0$$

$$\frac{D\rho}{Dt} = -\rho\nabla\cdot\mathbf{u}$$

with

$$\mathbf{u} = (u^1, u^2, u^3)\ , \qquad \mathbf{g} = (0, 0, -g)$$

Governing equations in Lagrangian form

Transformed governing PDEs in $\mathbf{S}_t$ (e.g. Clark JCP 1977, Prusa et al. JCP 2003):

$$\frac{du^j}{d\overline{t}} = -c_p\theta\tilde{G}_j^k\frac{\partial\pi}{\partial\overline{x}^k} - g\delta_3^j + M^j \qquad j = 1,2,3$$

$$\frac{d\theta}{d\overline{t}} = 0$$

$$\frac{d\rho}{d\overline{t}} = -\frac{\rho}{\overline{G}}\left(\frac{\partial\overline{G}\overline{v}^{s\,k}}{\partial\overline{x}^k}\right)$$

with

$$\frac{d}{d\overline{t}} = \frac{\partial}{\partial\overline{t}} + \overline{v}^{*\,k}\frac{\partial}{\partial\overline{x}^k}\ , \qquad \tilde{G}_j^k := \sqrt{g^{jj}}\frac{\partial\overline{x}^k}{\partial x^j} \qquad \overline{G} = |\overline{g}_{jk}|^{1/2}$$

$$\overline{v}^{*\,j} = \frac{d\overline{x}^j}{d\overline{t}} = \overline{v}^{s\,j} + \frac{\partial\overline{x}^j}{\partial t} \qquad \overline{v}^{s\,j} = \frac{\partial\overline{x}^j}{\partial x^k}u^{*\,k} \qquad v^k = \sqrt{g_{kk}}u^{*\,k}$$

$\rightarrow$ see e.g. textbook by Zdunkowski and Bott 2003 for fundamentals

Transformed governing PDEs in $\mathbf{S}_t$:

$$\frac{\partial \rho^* u^j}{\partial \overline{t}} + \overline{\nabla} \cdot \left(\overline{\mathbf{v}}^* \rho^* u^j \right) = -\rho^* c_p \theta \tilde{G}_j^k \frac{\partial \pi}{\partial \overline{x}^k} - \rho^* g \delta_3^j + \rho^* M^j \qquad j = 1, 2, 3$$

$$\frac{\partial \rho^* \theta}{\partial \overline{t}} + \overline{\nabla} \cdot (\overline{\mathbf{v}}^* \rho^* \theta) = 0$$

$$\frac{\partial \rho^*}{\partial \overline{t}} + \overline{\nabla} \cdot (\overline{\mathbf{v}}^* \rho^*) = 0$$

with

$$\overline{\nabla} \equiv \left(\frac{\partial}{\partial \overline{x}}, \frac{\partial}{\partial \overline{y}}, \frac{\partial}{\partial \overline{z}} \right) , \qquad \overline{\mathbf{v}}^* \equiv \left(\overline{v}^{*1}, \overline{v}^{*2}, \overline{v}^{*3} \right) , \qquad \rho^* \equiv \overline{G} \rho$$

Tensor identities

1. Divergence in generalised coordinates:

$$\nabla \cdot \mathbf{A} = \frac{1}{\overline{G}} \frac{\partial}{\partial \overline{x}^k} \left(\overline{G}\, \overline{A}^k \right) - \overline{A}^j \left[\frac{G}{\overline{G}} \frac{\partial}{\partial \overline{x}^k} \left(\frac{\overline{G}}{G} \frac{\partial \overline{x}^k}{\partial x^j} \right) \right]$$

Invariance of divergence uses multi-component geometric conservation law (GCL):

$$\frac{G}{\overline{G}} \frac{\partial}{\partial \overline{x}^k} \left(\frac{\overline{G}}{G} \frac{\partial \overline{x}^k}{\partial x^j} \right) \equiv 0$$

2. Reciprocity of covariant and contravariant base vectors:

$$\overline{\mathbf{q}}^r \cdot \overline{\mathbf{q}}_s = \frac{\partial \overline{x}^r}{\partial x^q} \frac{\partial x^q}{\partial \overline{x}^s} = \delta^r_s$$

$\rightarrow$ Discrete model should respect these identities ! (see e.g. Thomas and Lombard 1979, Prusa and Gutowski IJNMF 2006, Kühnlein et al. JCP 2012)

Vertical coordinates in atmospheric models

→ Independent vertical variable ζ

$$(\overline{x}, \overline{y}, \zeta) = (x, y, \zeta(t, x, y, z))$$

- height z
- (hydrostatic) pressure p
- potential temperature θ
- ...

→ Terrain-following coordinates

- \+ levels do not intersect the earth's surface
- \+ specification of the lower boundary condition
- \+ uniform vertical mesh spacing near the surface
- \+ stretching easily allows higher resolution towards the surface
- \+ long time steps
- (-) potential errors in pressure gradient term
- (-) mesh quality for steep orography

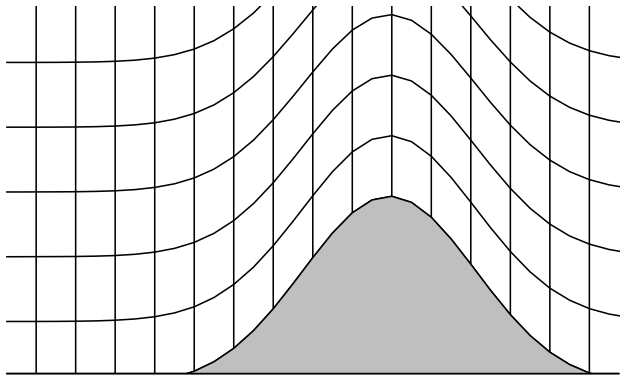

Gal-Chen and Somerville terrain-following vertical coordinate

Terrain-following coordinate of Gal-Chen and Somerville (1975):

$$\overline{z} = \overline{z}(x, y, z) = H \frac{z - h(x, y)}{H - h(x, y)}$$

with inverse mapping

$$z = z(x, y, \overline{z}) = \overline{z} + \left(1 - \frac{\overline{z}}{H}\right) h = \overline{z} + b(\overline{z}) h(x, y)$$

H: height of model top

$h(x, y)$: local height of orography

$b(\overline{z})$: vertical decay function of orography

Gal-Chen and Somerville terrain-following vertical coordinate

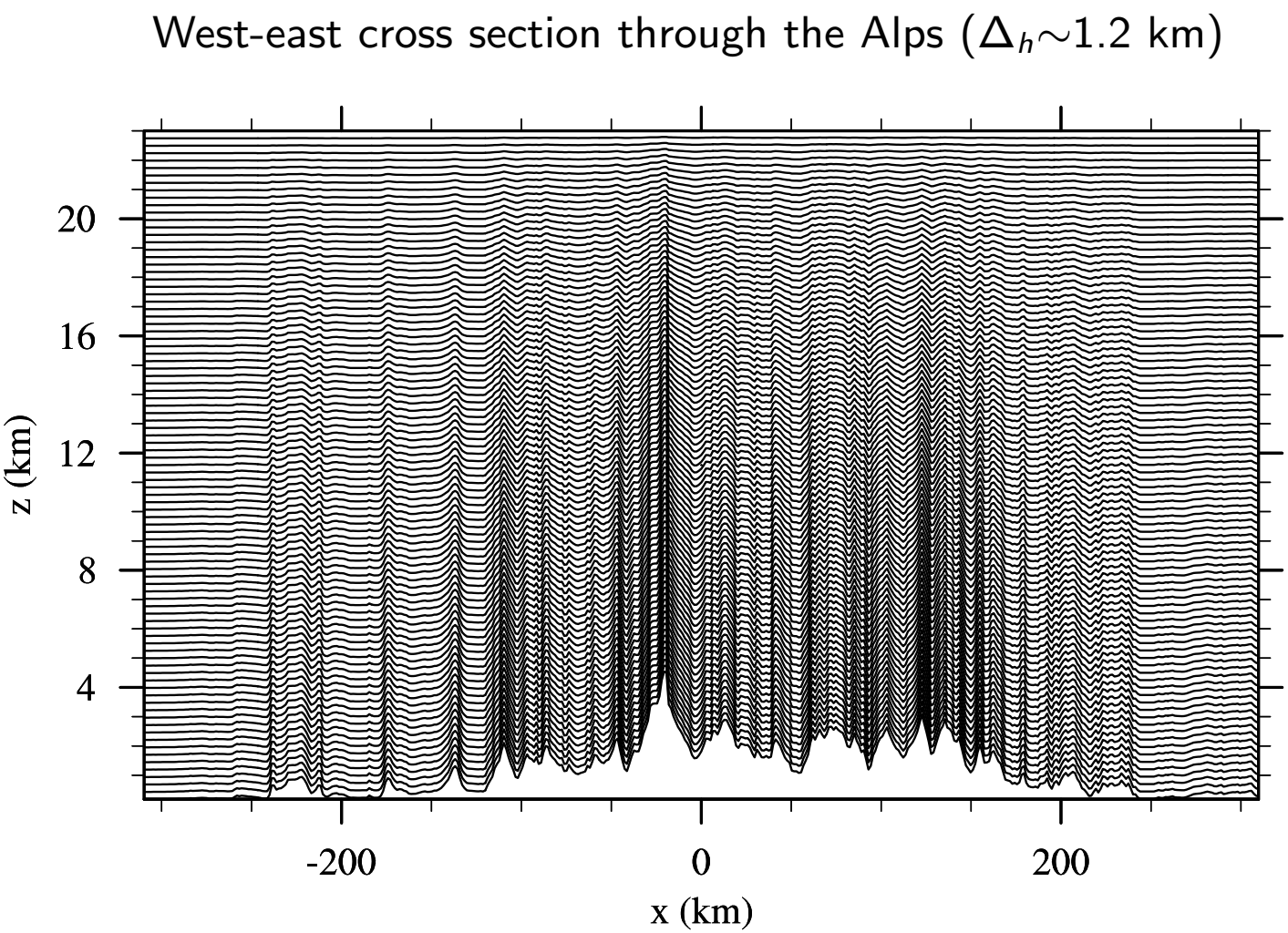

Gal-Chen and Somerville terrain-following vertical coordinate

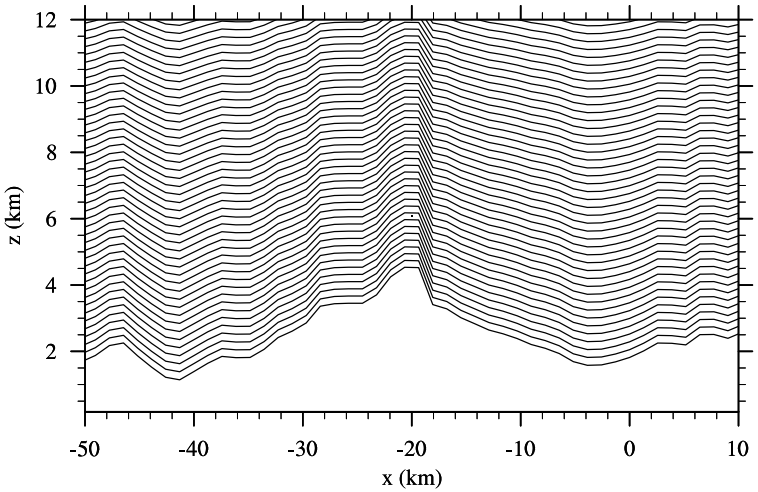

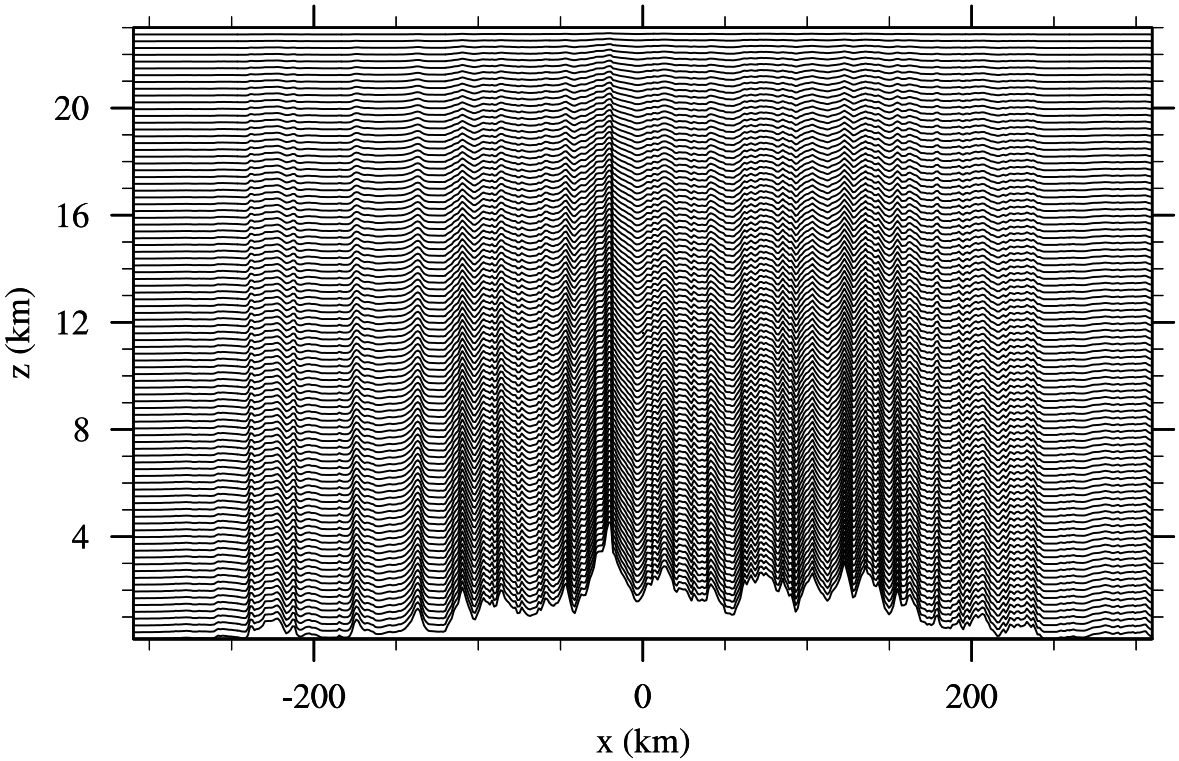

Gal-Chen and Somerville terrain-following vertical coordinate

Hybrid specification:

$$z(x, y, \overline{z}) = \overline{z} + b(\overline{z})h(x, y)$$

where

$$b(\overline{z}) = \begin{cases} (1 - \overline{z}/H_r) & : \overline{z} \leq H_r \\ 0 & : \overline{z} > H_r \end{cases}$$

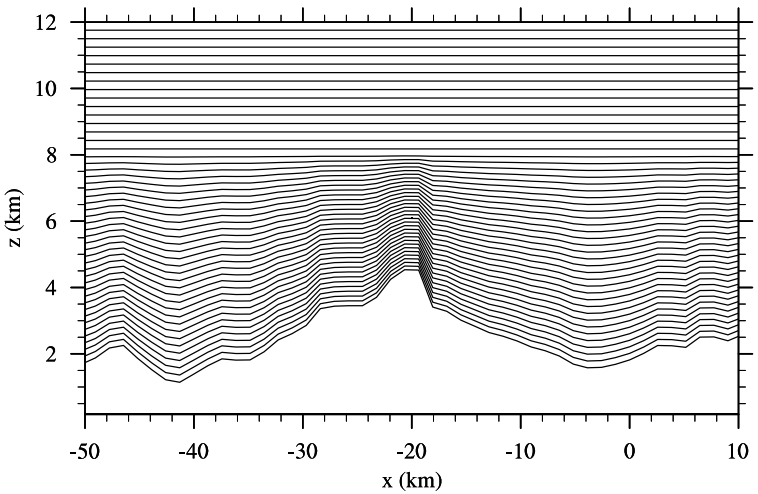

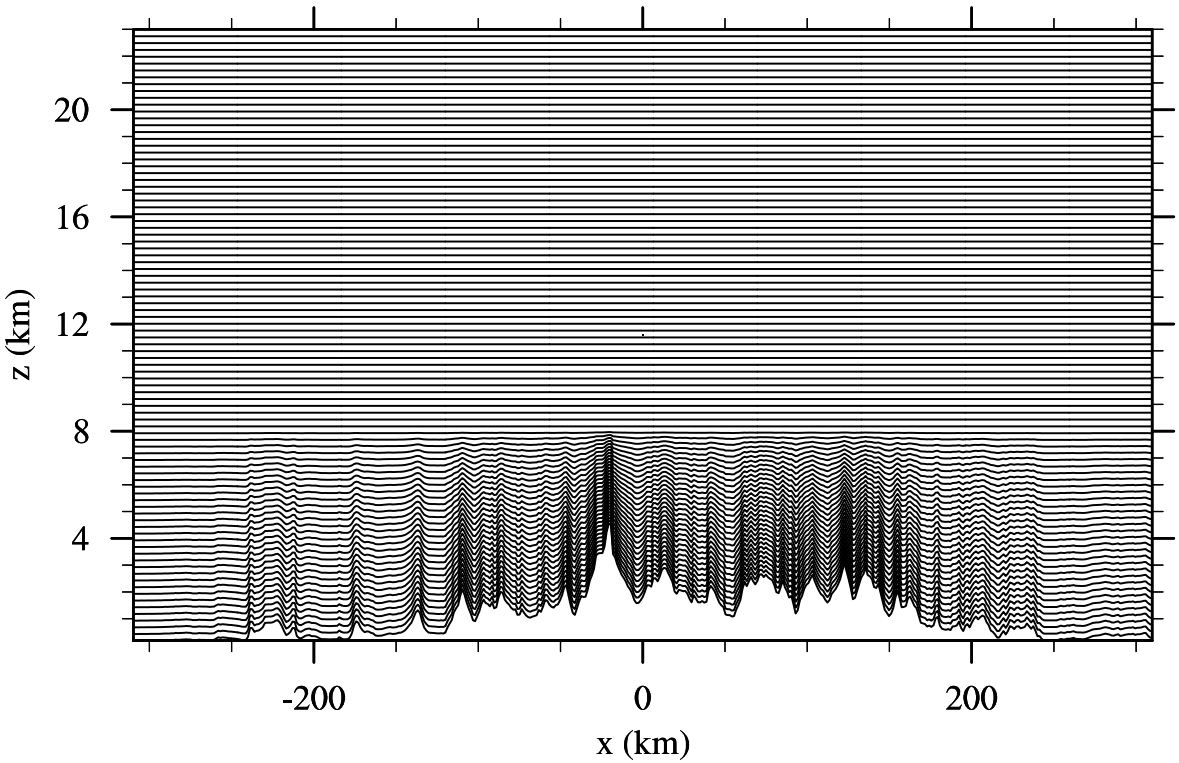

Smoothed height-based terrain-following coordinates

Smoothed coordinate – SLEVE (Schär et al. MWR 2002, Leuenberger et al. MWR 2010):

$$z(x, y, \overline{z}) = \overline{z} + b_s h_s(x, y) + b_r h_r(x, y)$$

h_s : smoothed terrain
$h_r = h - h_s$: residual containing small-scale variations of terrain
b_s : vertical decay function for h_s
b_r : vertical decay function for h_r
with

$$b_i(\overline{z}) = \frac{\sinh\left[(H/s_i)^n - (\overline{z}/s_i)^n\right]}{\sinh\left[(H/s_i)^n\right]}$$

$\Rightarrow$ Faster decay for b_r versus b_s by defining smaller scale-height s_i

See also: Zängl MWR 2003, Klemp MWR 2011

SLEVE coordinate

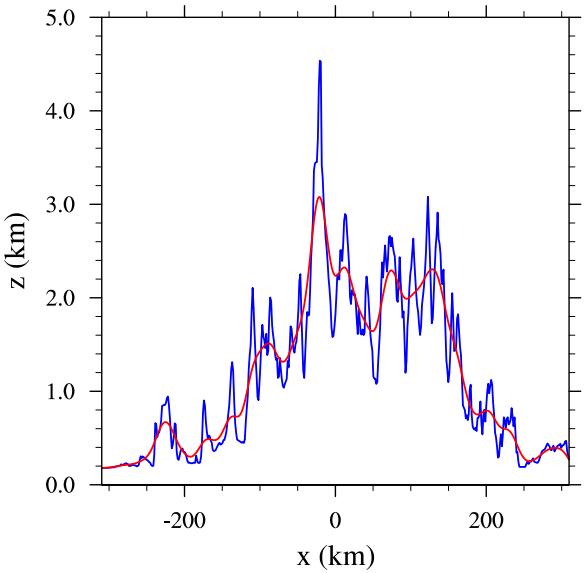

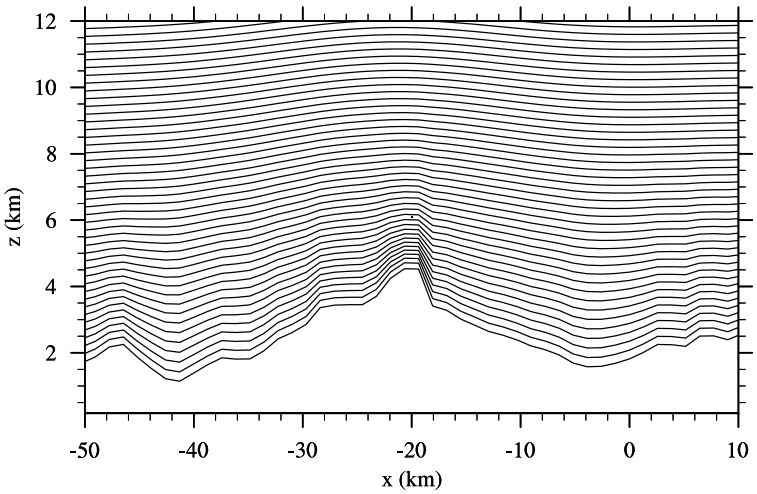

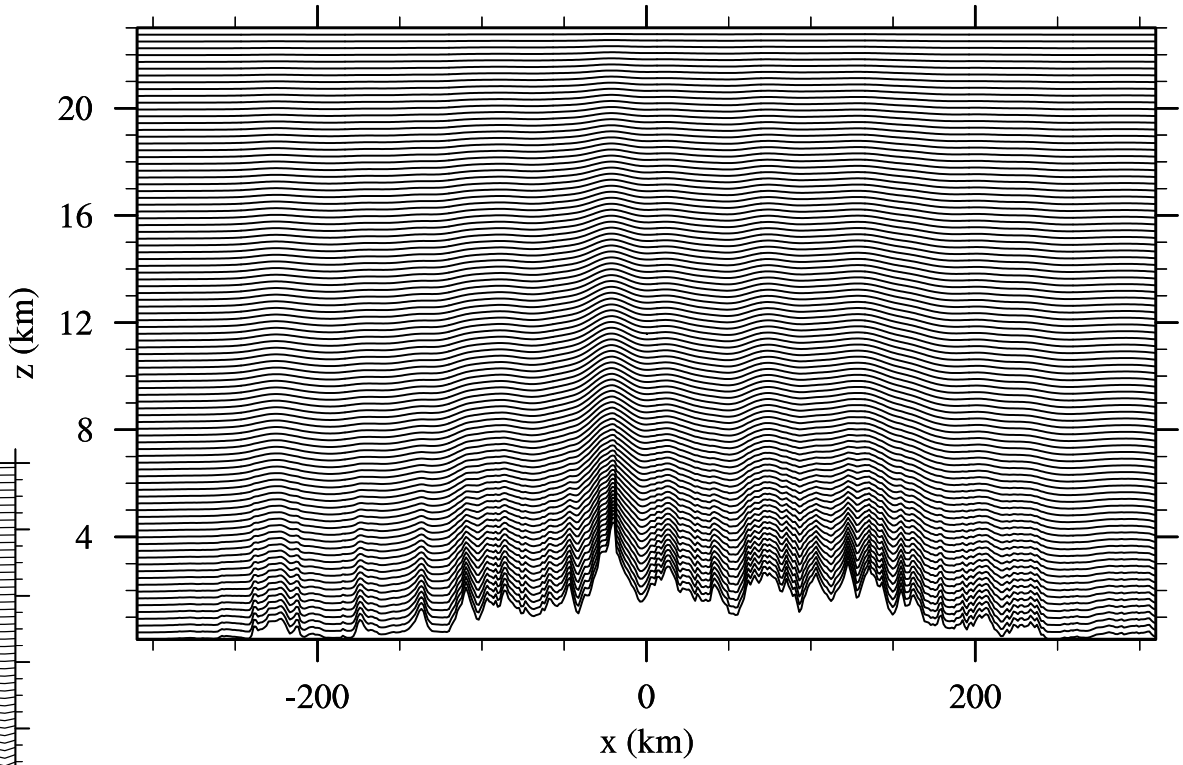

SLEVE coordinate

SLEVE in hybrid setting with vertical stretching:

$$\tilde{z} = C^{-1}(\bar{z}) \quad \rightarrow \quad z = z(x, y, \tilde{z})$$

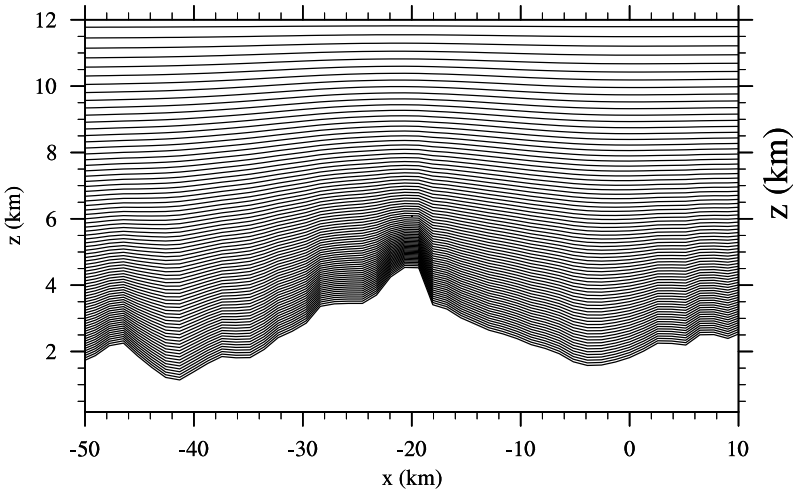

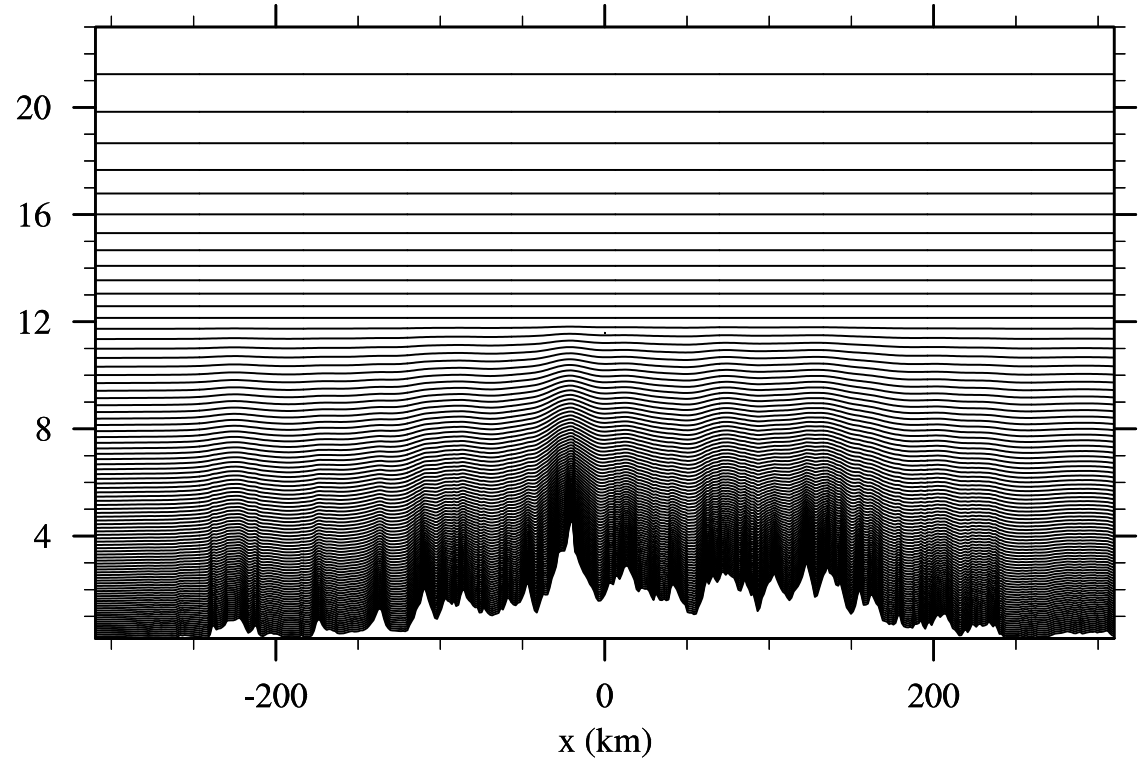

Pressure-based terrain-following coordinates

Pressure-based terrain-following vertical coordinate η of the form:

$$(\overline{x}, \overline{y}, \eta) \equiv (x, y, \eta(p, p_s))$$

with $\eta_s = \eta(p_s, p_s) \equiv 1$ $\eta_t = \eta(p_t, p_s) \equiv 0$

$p(t, x, y, z)$: pressure, $p_s(t, x, y)$: surface pressure, p_t: top pressure
$\rightarrow$ bijective mapping between p and η for a given p_s.

One example is (Phillips JM 1957 "A coordinate system having some special advantages for numerical forecasting", Mintz 1965)

$$\sigma = \eta = \frac{p - p_t}{p_s - p_t}$$

commonly named as the σ-coordinate.

Hybrid pressure-based terrain-following coordinates

Hybrid σ-p vertical coordinate (Simmons and Burridge MWR 1981) employed in ECMWF's operational IFS model (with $p_t \equiv 0$):

$$p(t, x, y, z) = A(\eta) + B(\eta) p_s(t, x, y)$$

with

$$A(\eta_t) = 0 \ , \quad B(\eta_t) = 0 \ , \quad A(\eta_s) = 0 \ , \quad B(\eta_s) = 1$$

$\rightarrow$ terrain-following σ-like levels near the earth's surface with transition to pressure levels in the upper troposphere and stratosphere

- different approaches to specify A and B coefficients (see e.g. Eckermann MWR 2009)
- similar in non-hydrostatic models (Laprise MWR 1992, Bubnova et al. MWR 1995)

Hybrid pressure-based terrain-following coordinates

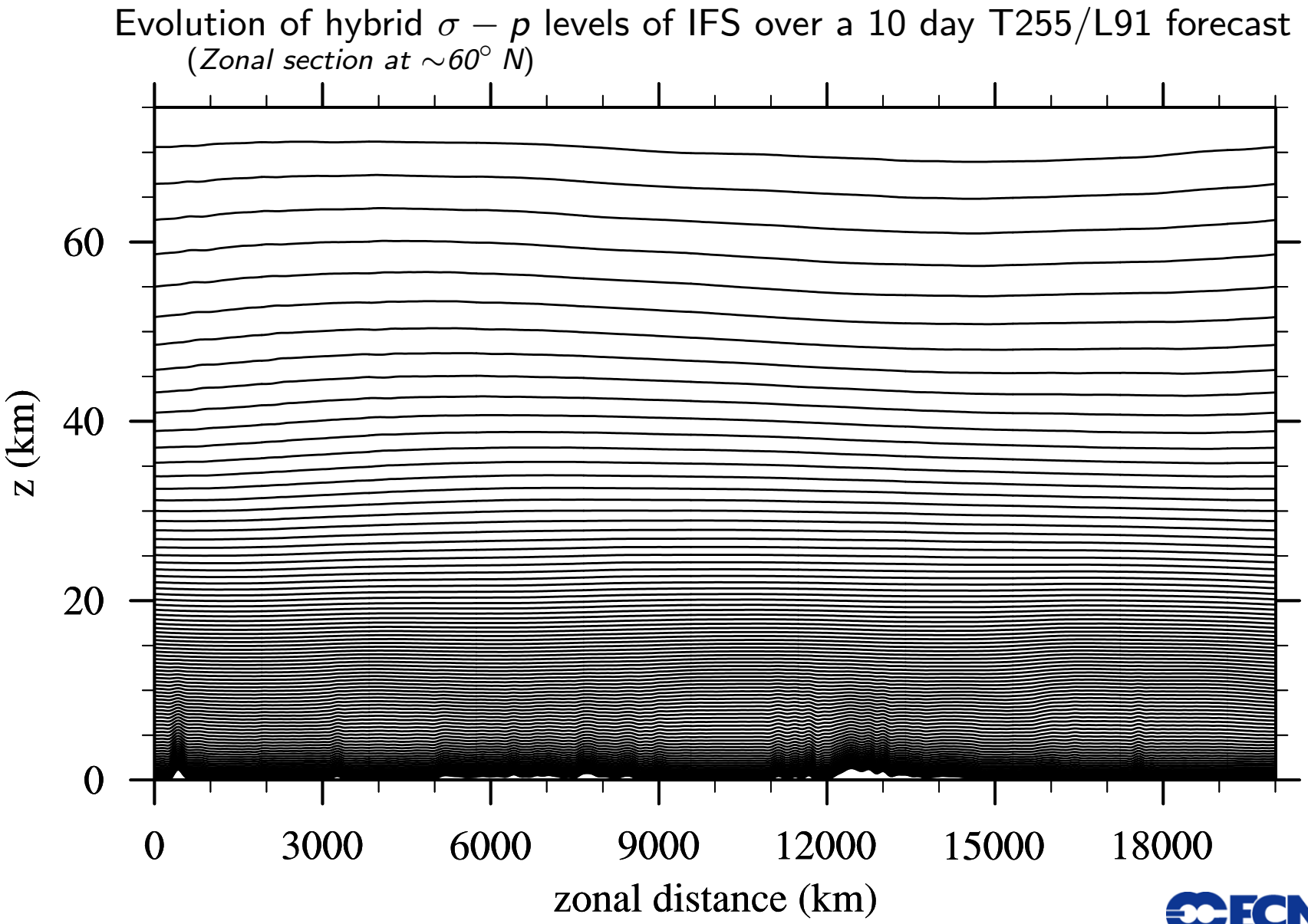

Isentropic vertical coordinates

Potential temperature θ as independent vertical coordinate:

- for inviscid adiabatic flow $D\theta/Dt = 0$ isentropes represent material surfaces
- more accurate representation of vertical transport
- adaptive vertical mesh spacing proportional to thermal stratification
- implemented as hybrid terrain-following-θ coordinate
- becomes more complicated for high resolution due to small-scale θ variations
- regularisation of coordinate required to ensure monotonicity

$\rightarrow$ see e.g. Hsu and Arakawa, MWR 1990; Konor and Arakawa, MWR 1997; Benjamin et al. MWR 2004; Toy and Randall MWR 2009

Pressure gradient term with terrain-following coordinates

$\Rightarrow$ horizontal pressure gradient

$$-c_p\theta\frac{\partial\pi}{\partial x} = -c_p\theta\left(\frac{\partial\pi}{\partial\overline{x}} + \frac{\partial\overline{z}}{\partial x}\frac{\partial\pi}{\partial\overline{z}}\right)$$

susceptible to errors

+ subtraction of balanced state
+ satisfy tensor identities, consistency of discrete metrics and dynamics (see e.g. Prusa and Gutowski IJNMF 2006; Klemp et al. MWR 2003)
+ boundary conditions (e.g. Smolarkiewicz et al. JCP 2007)
+ smoothed coordinate levels
+ truly horizontal evaluation of horizontal components of the pressure gradient and horizontal diffusion using reconstructed quantities on Cartesian mesh (Zängl MWR 2012, and references therein)
+ see also Lin QJ 1996, Weller and Shahrokhi MWR 2014

Steep orography with a basic terrain-following vertical coordinate

Stratified flow past isolated mountain with FVM (max. slope $\sim 37^\circ$)

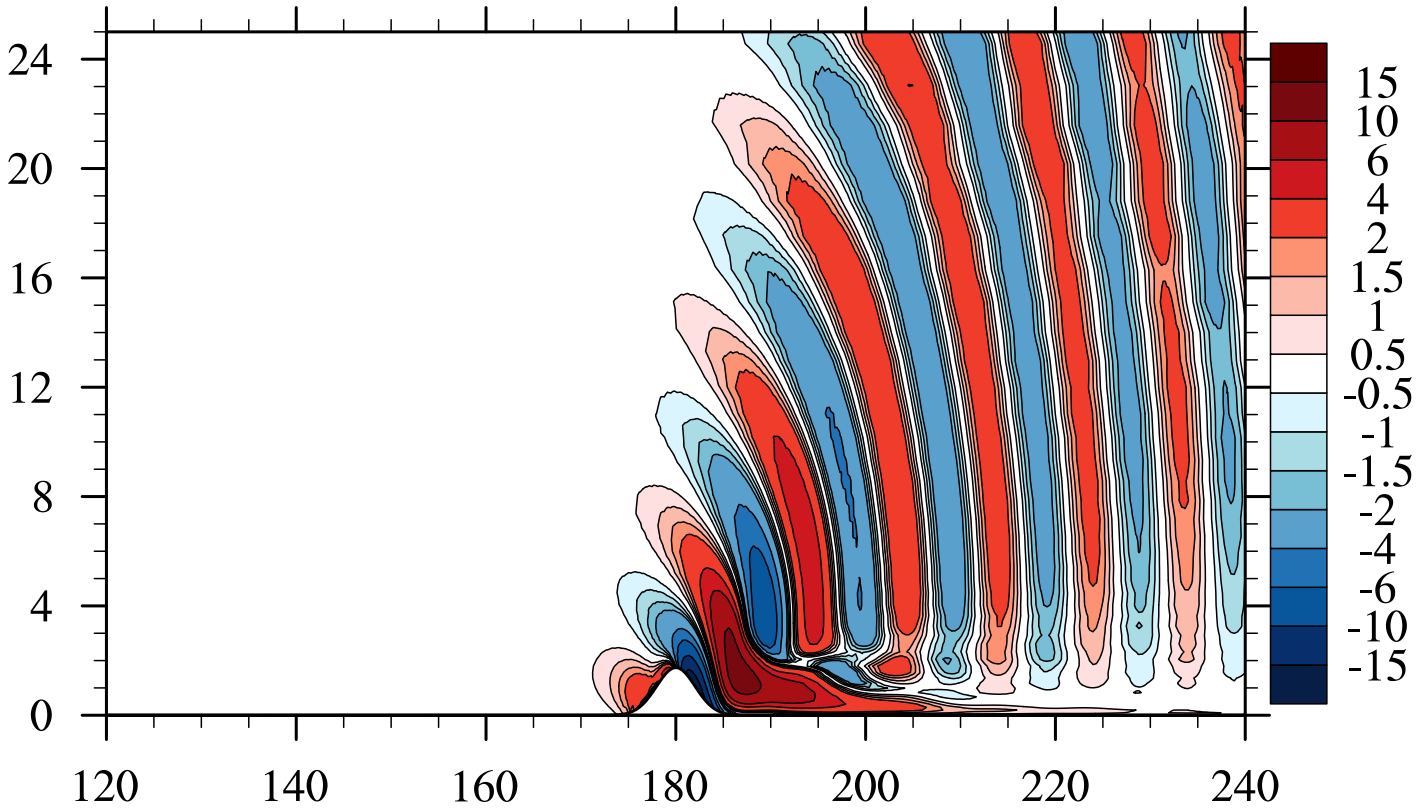

$\rightarrow$ Basic terrain-following coordinate, semi-implicit integration of Euler equations (Smolarkiewicz et al. 2014), finite-volume MPDATA scheme (Kühnlein and Smolarkiewicz 2017), no explicit diffusion

Steep orography with a basic terrain-following vertical coordinate

Stratified flow past isolated mountain with FVM (max. slope $\sim 71^\circ$)

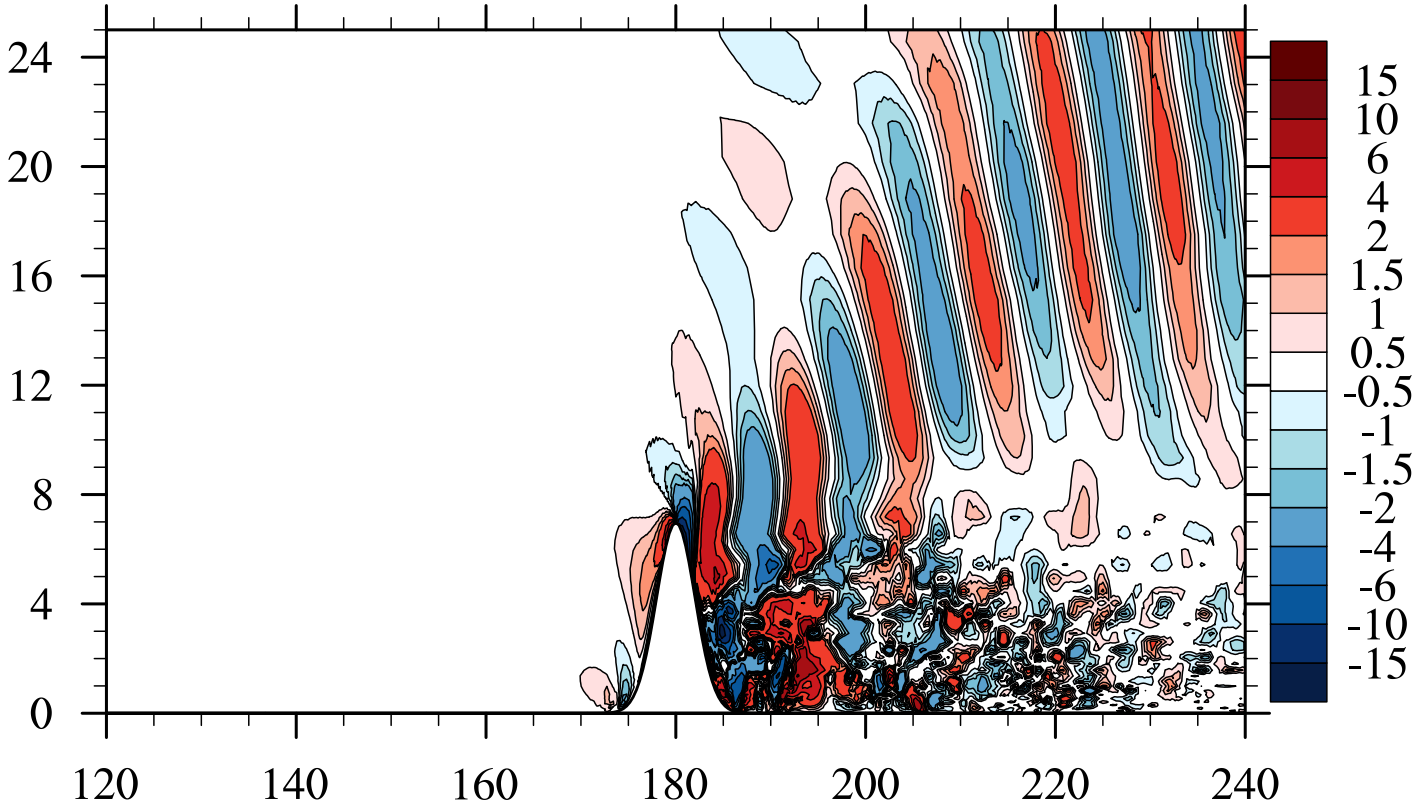

$\rightarrow$ Basic terrain-following coordinate, semi-implicit integration of Euler equations (Smolarkiewicz et al. 2014), finite-volume MPDATA scheme (Kühnlein and Smolarkiewicz 2017), no explicit diffusion

Other techniques

→ Cut-cell method (e.g. Steppeler et al. 2002, Klein et al. 2009, Lock et al. 2012)

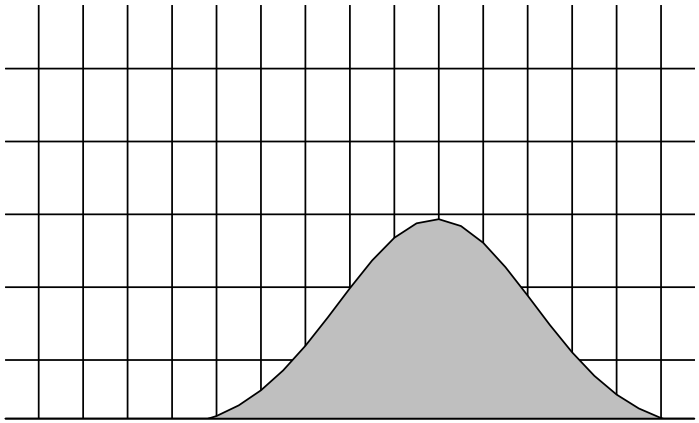

Other techniques

→ Slanted cell approach (Shaw and Weller MWR 2016, Shaw et al. 2017)

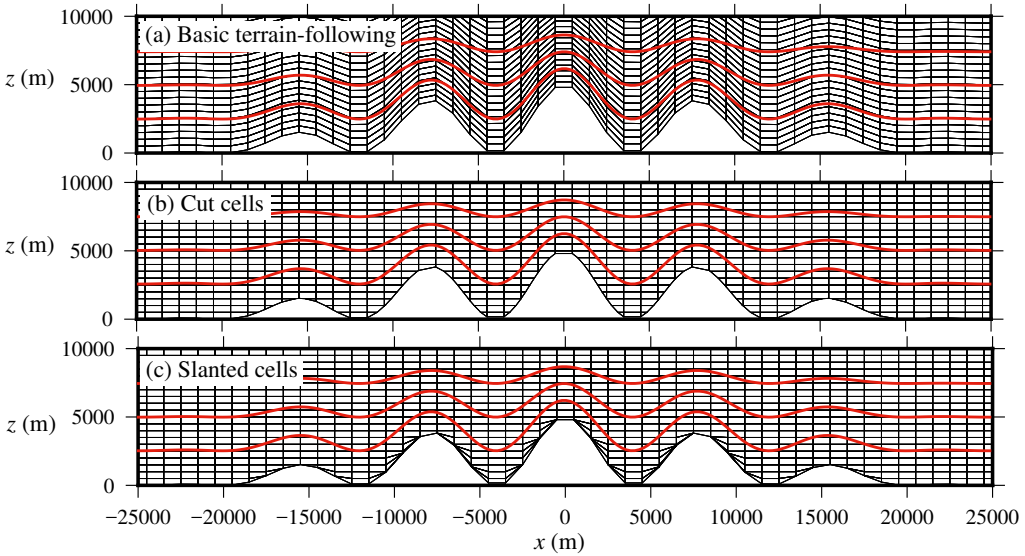

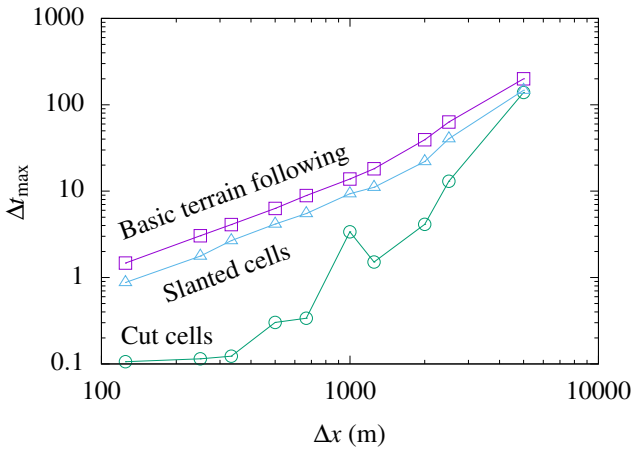

Other techniques

→ 3D unstructured mesh discretisation → see J. Szmelter's lecture

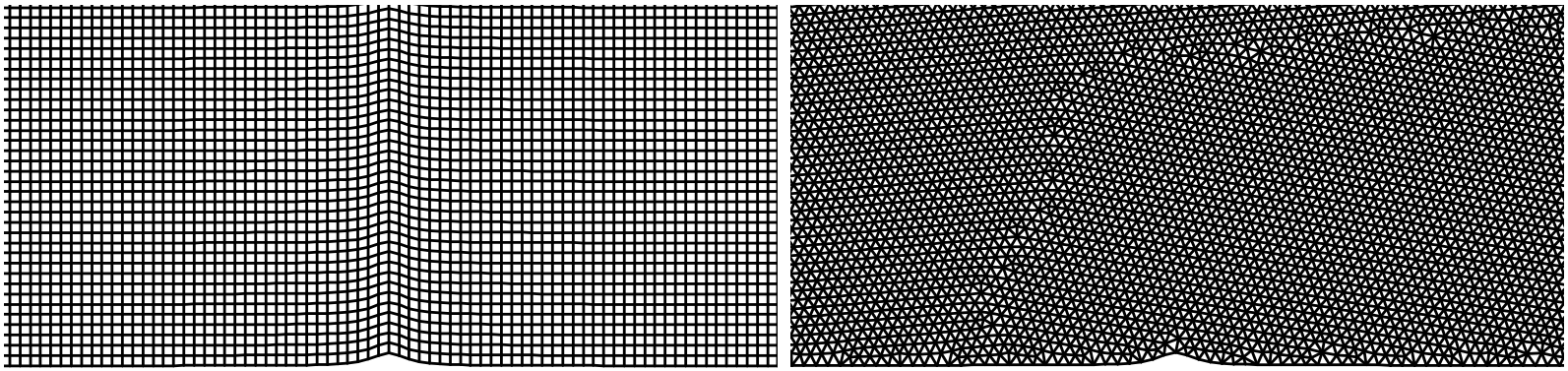

Multiscale atmospheric flows

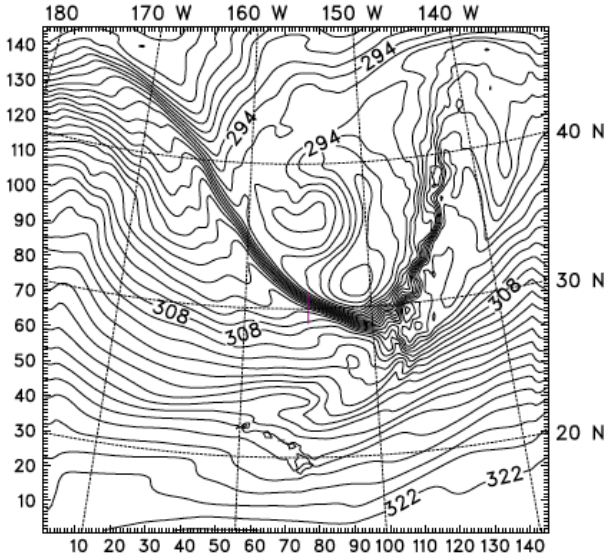

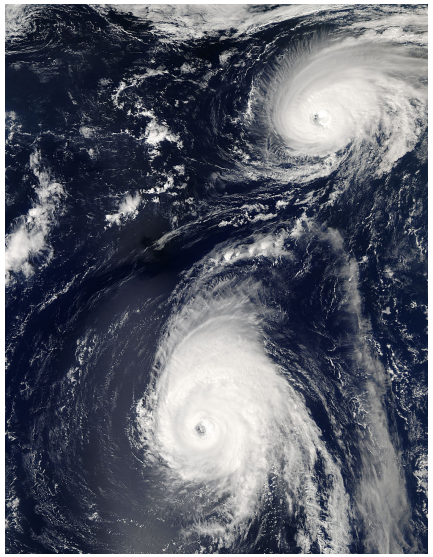

→ Extremely different local scales in atmospheric flows

→ Standard approach in atmospheric solvers of uniform mesh not optimal

→ Variable mesh applying locally finer/coarser spacing more efficient

→ Solution-adaptive mesh is able to conform to flow evolution

$$(\overline{x}, \overline{y}) = (E(t, x, y), D(t, x, y)) : \quad \mathcal{D}_p \to \mathcal{D}_t$$

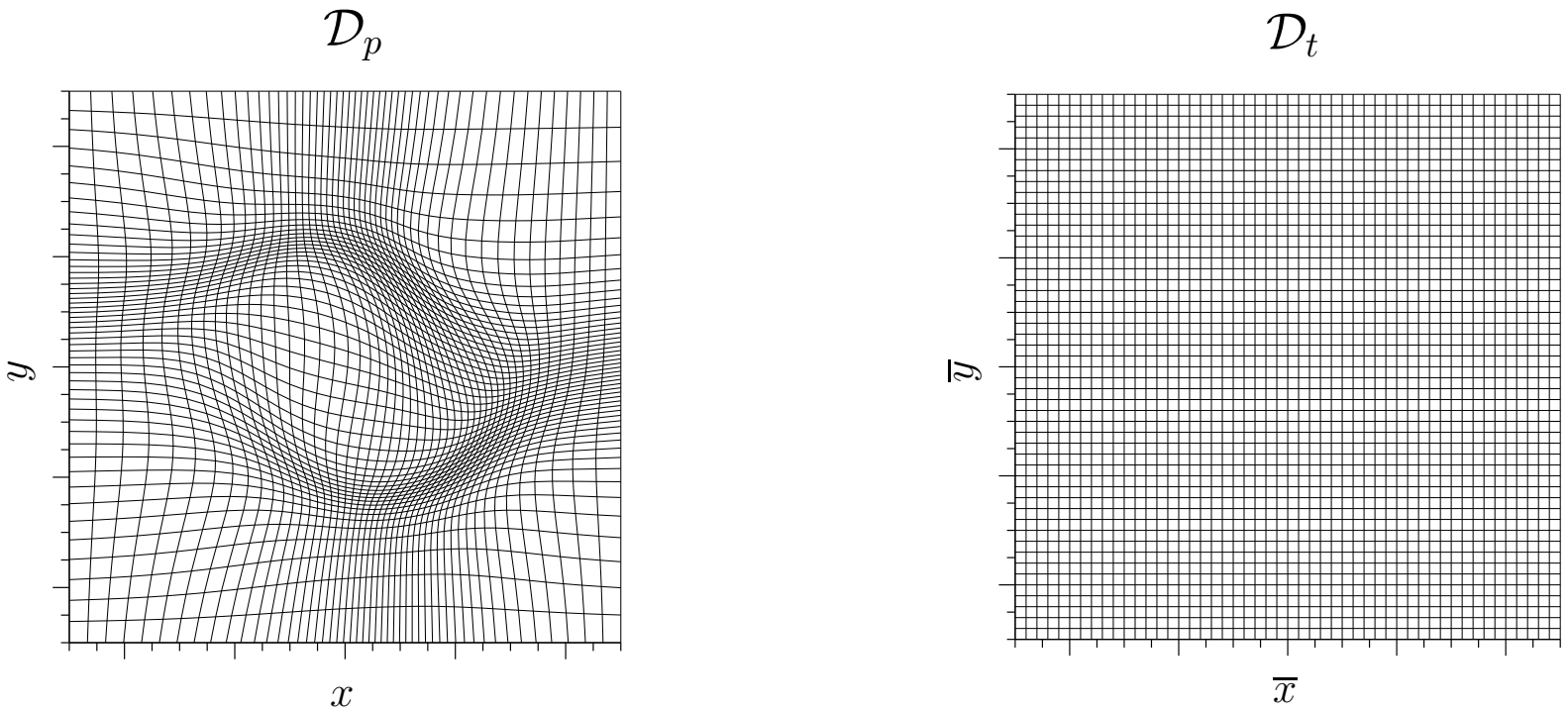

$\rightarrow$ moving mesh or r-adaptive technique (see Budd et al. AN 2009 for comprehensive discussion)

Scalar advection experiment

Time-dependent deformational shear flow (Blossey and Durran, JCP 2008) using advection scheme MPDATA (Smolarkiewicz IJNMF 2006) with moving meshes (Kühnlein et al. JCP 2012):

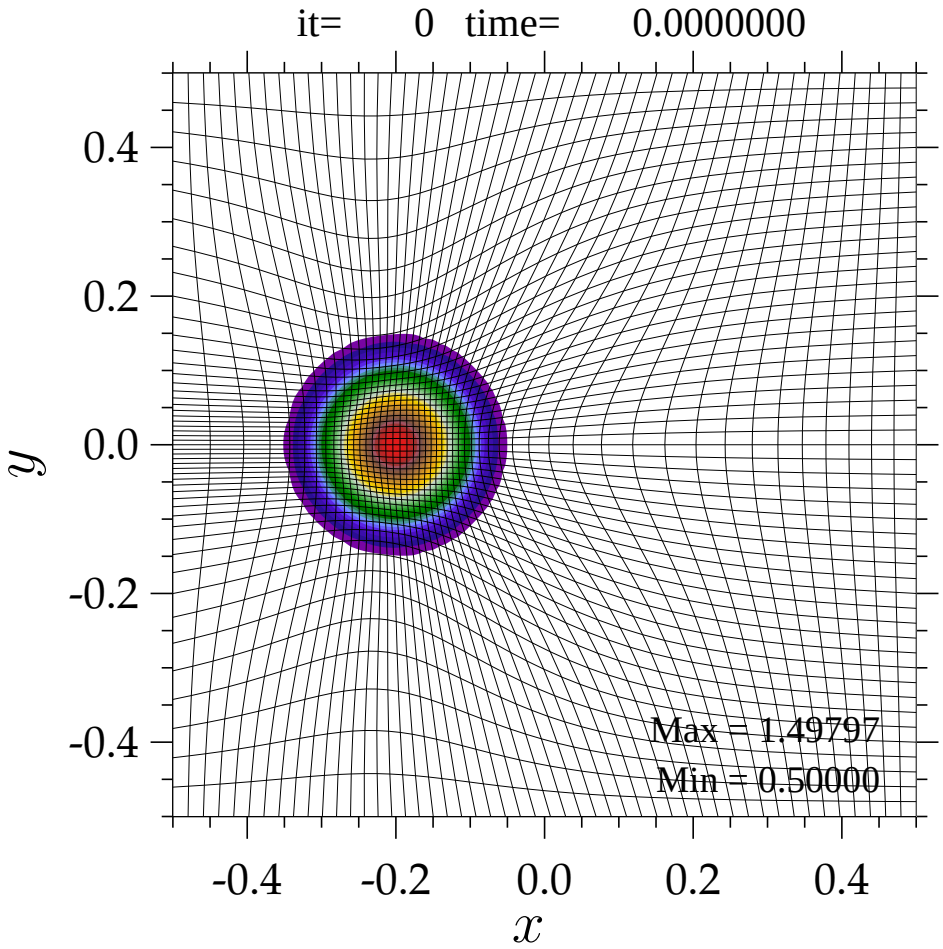

$\rightarrow$ mesh refinement indicator: $\Phi = ||\nabla\psi||$

Scalar advection experiment

uniform mesh - 50^2, $T_{rw} = 1$

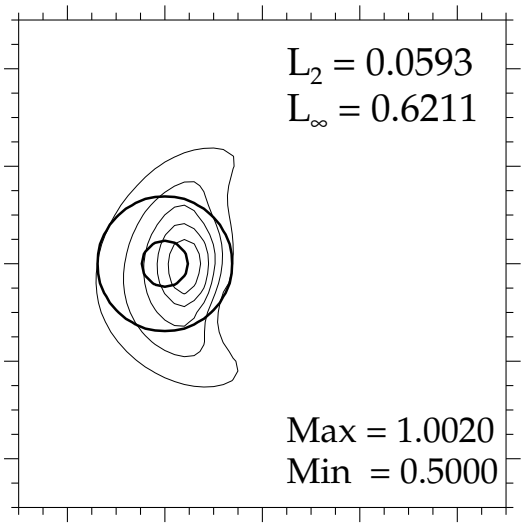

uniform mesh - 250^2, $T_{rw} = 133$

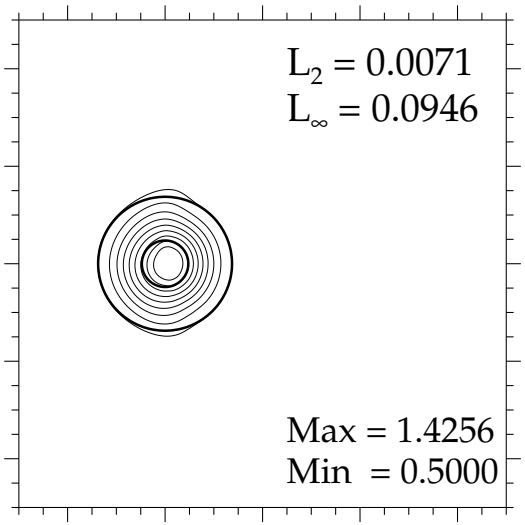

adaptive mesh - 50^2, $T_{rw} = 5.5$

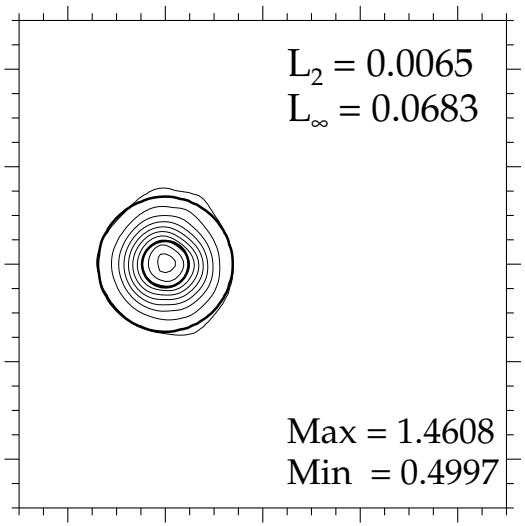

$\rightarrow$ T_{rw} is relative wall clock time to uniform mesh run with 50^2 mesh cells (leftmost panel)

MMPDEs (Huang JCP 2001) govern time-dependent mapping (here 2D) from computational to physical space:

$$P(\mathbf{x}_h, M)\,\frac{\partial \mathbf{x}_h}{\partial \overline{t}} = \sum_{i,j=1,2} D_{ij}(\mathbf{x}_h, M)\,\frac{\partial^2 \mathbf{x}_h}{\partial \overline{x}^i \partial \overline{x}^j} + \sum_{i=1,2} C_i(\mathbf{x}_h, M)\,\frac{\partial \mathbf{x}_h}{\partial \overline{x}^i}$$

with coefficients

$$D_{ij}(\mathbf{x}_h, M) = \nabla_h\,\overline{x}^i \cdot M^{-1}\,\nabla_h\,\overline{x}^j\ , \qquad C_i(\mathbf{x}_h, M) = -\nabla_h\,\overline{x}^i \cdot \left(\sum_{k=1,2} \frac{\partial M^{-1}}{\partial \overline{x}^k}\,\nabla_h\,\overline{x}^k\right)\ ,$$

$$P(\mathbf{x}_h, M) = \mathcal{T}\,\sqrt{(D_{11})^2 + (D_{22})^2 + (C_1)^2 + (C_2)^2}$$

$\Rightarrow$ MMPDEs are derived from variational principles as a minimiser of mapping functional

$$\mathcal{I}[\overline{\mathbf{x}}] = \frac{1}{2}\int_{\mathcal{D}_p} \sum_{k=1}^{2} (\nabla \overline{x}^k)^T\, M^{-1}\,\nabla \overline{x}^k\, d\mathbf{x}$$

One-dimensional stationary view on the MMPDE:

$$\mathcal{I}[\overline{x}] = \frac{1}{2} \int_{\mathcal{D}_p} \frac{1}{m} \left(\frac{\partial \overline{x}}{\partial x} \right)^2 dx$$

with Euler-Lagrange equation

$$\frac{\partial}{\partial \overline{x}} \left(m(x) \frac{\partial x}{\partial \overline{x}} \right) = 0 \ + \text{BCs}$$

$m(x) : \mathbf{S}_p \to \mathbb{R}^+$ is monitor function to control local mesh spacing

Moving mesh PDEs

- Example:

$x(0) = 0, \quad x(1) = 1$
$\overline{x}(0) = 0, \quad \overline{x}(1) = 1$

$m(x) = 1$

$$\frac{\partial}{\partial \overline{x}} \left(m(x) \frac{\partial x}{\partial \overline{x}} \right) = 0$$

$$\Rightarrow \quad x = x(\overline{x})$$

Number of grid increments: N =20

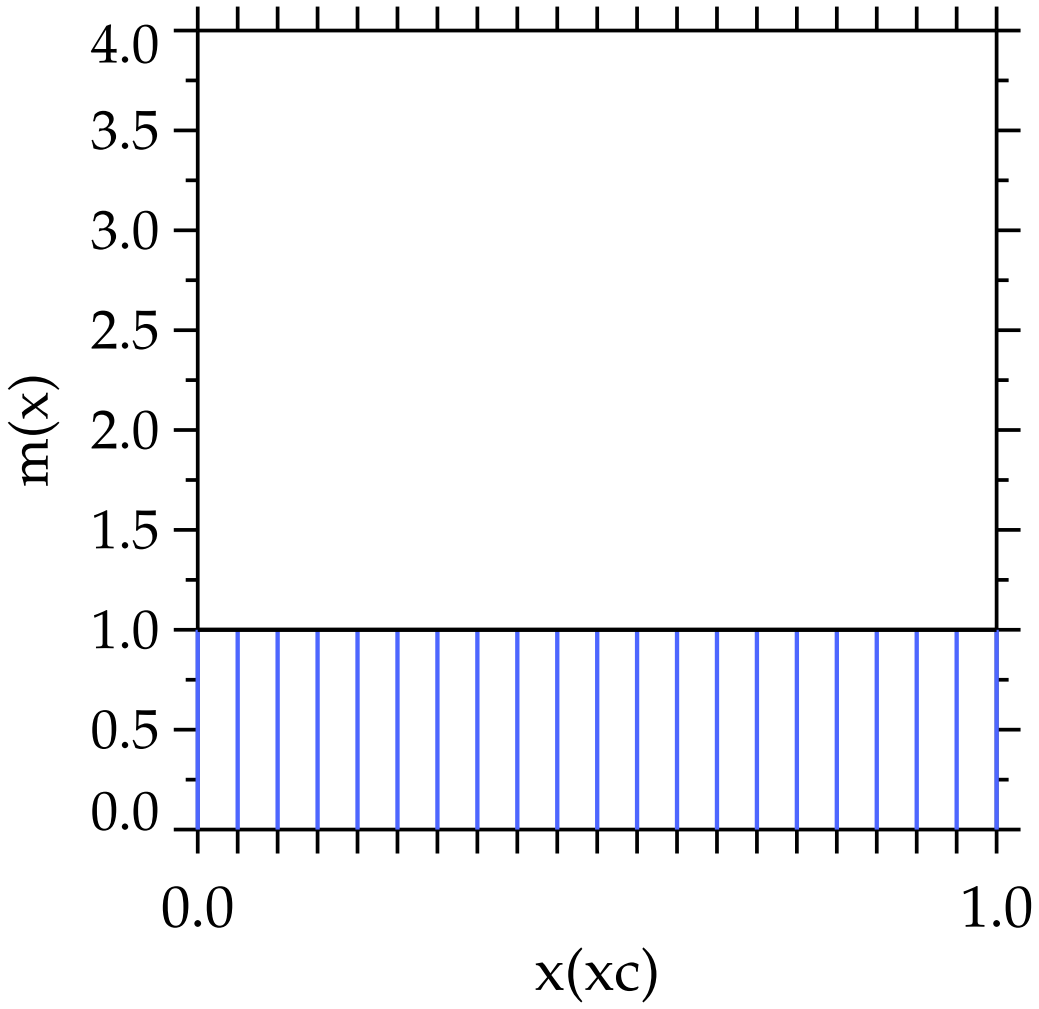

Moving mesh PDEs

- Example:

$x(0) = 0, \quad x(1) = 1$
$\overline{x}(0) = 0, \quad \overline{x}(1) = 1$

$m(x) = \exp(x \ln 2)$

$$\frac{\partial}{\partial \overline{x}} \left(m(x) \frac{\partial x}{\partial \overline{x}} \right) = 0$$

$$\Rightarrow \quad x = x(\overline{x})$$

Number of grid increments: N =20

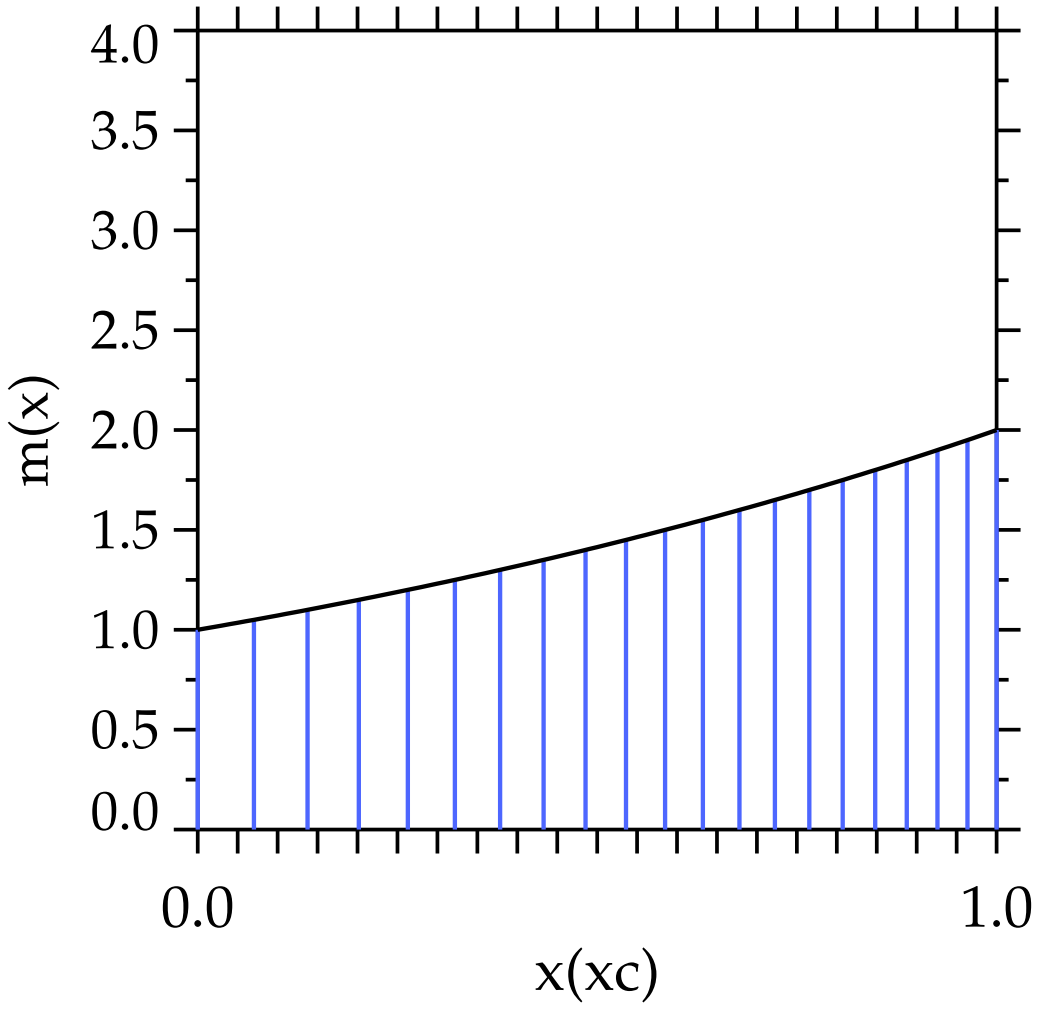

Moving mesh PDEs

- Example:

$x(0) = 0, \quad x(1) = 1$
$\overline{x}(0) = 0, \quad \overline{x}(1) = 1$

$m(x) = \exp(x \ln 4)$

$$\frac{\partial}{\partial \overline{x}} \left(m(x) \frac{\partial x}{\partial \overline{x}} \right) = 0$$

$$\Rightarrow \quad x = x(\overline{x})$$

Number of grid increments: N =20

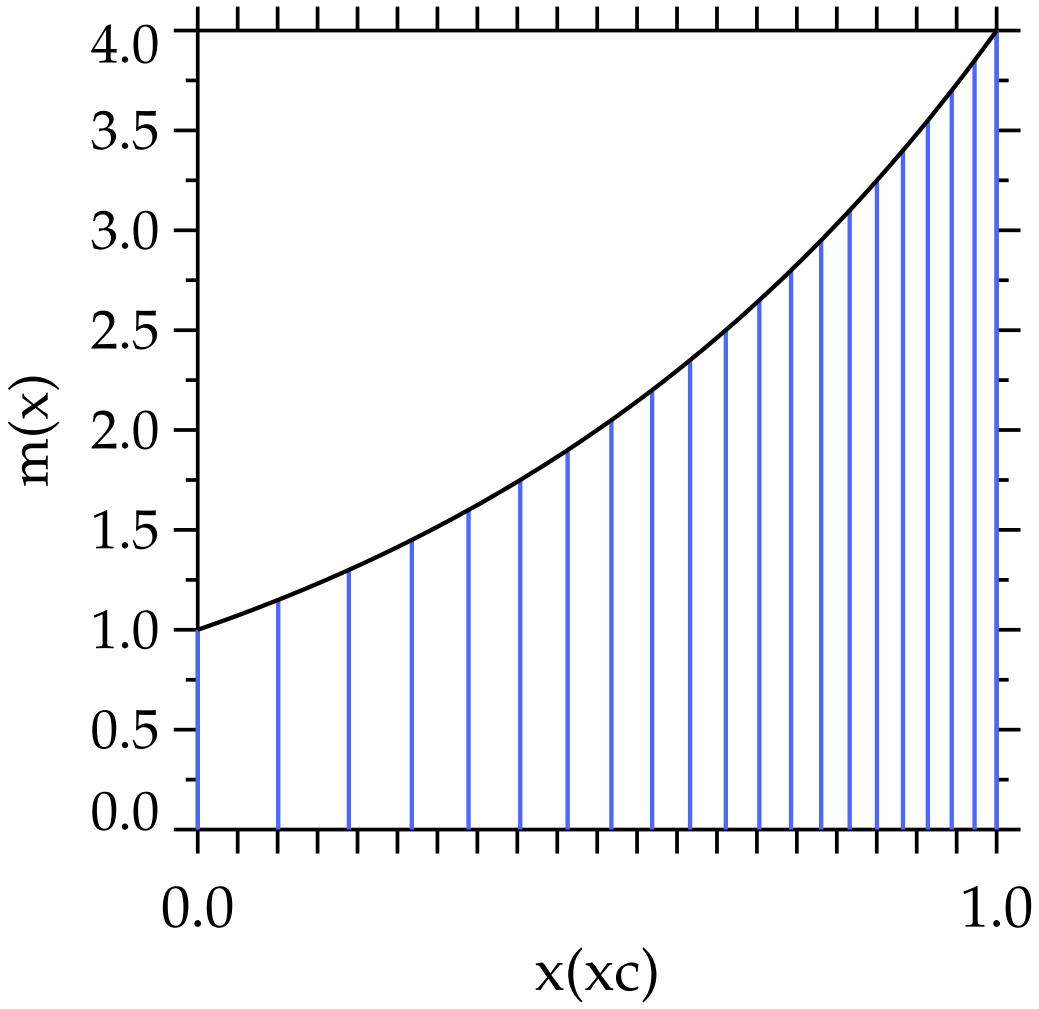

Moving mesh PDEs

→ Monitor function M (2×2 matrix in 2D):

$$M = I\, q$$

with scalar weighting function

$$q(t, \mathbf{x}_h) = 1 + \frac{\beta}{1-\beta}\,\frac{\Phi}{\langle \Phi \rangle_h}\,, \qquad I \text{ is identity matrix}$$

→ Φ is mesh refinement indicator; $\langle \Phi \rangle_h$ denotes its horizontal average

→ $0 \leq \beta < 1$ controls strength of adaptation

→ q is filtered to obtain good quality mesh

→ boundary conditions of 2D MMPDEs are either of Dirichlet-type for $\mathbf{x}_h$ found by means of 1D MMPDEs

$$p(s, \mu)\,\frac{\partial s}{\partial \bar{t}} = \mu\,\frac{\partial^2 s}{\partial \bar{s}^2} + \frac{\partial \mu}{\partial \bar{s}}\,\frac{\partial s}{\partial \bar{s}}$$

along boundary segments or are assumed periodic, depending on BC of the model

Adaptive moving mesh solver

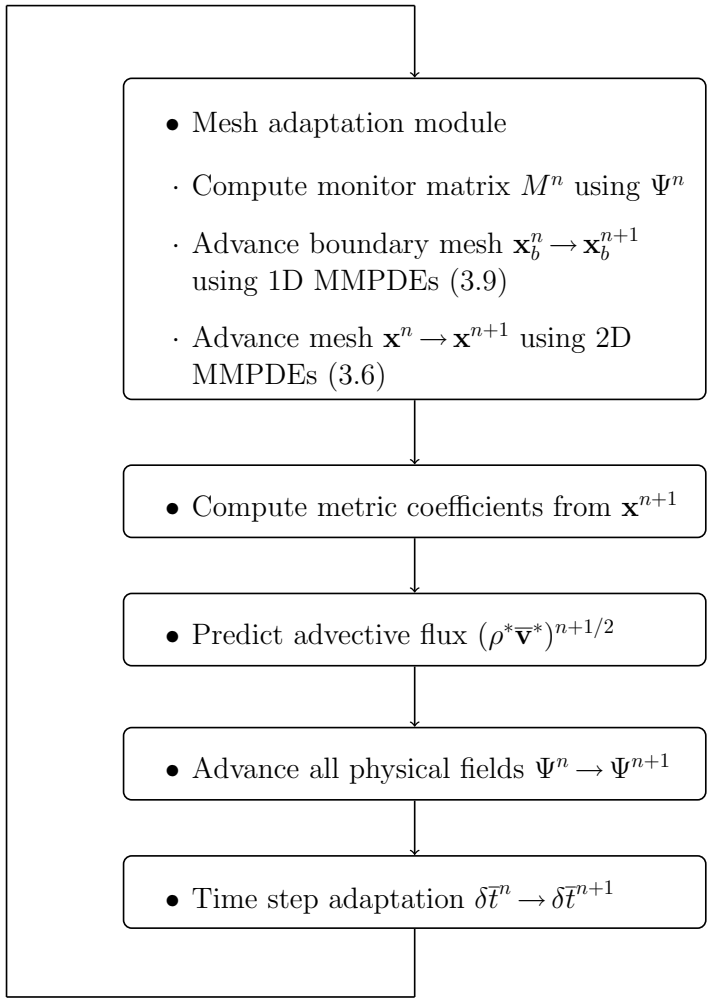

· In framework of two-time-level flow solver EULAG (Prusa et al. CF 2008, Kühnlein et al. JCP 2012)

Adaptive simulation of convective bubble

Combining the soundproof and compressible PDE solver (Smolarkiewicz et al. JCP 2014) with adaptive moving meshes:

$$(\overline{x}, \overline{z}) = (E(t, x, z), D(t, x, z)) : \quad \mathcal{D}_p \to \mathcal{D}_t$$

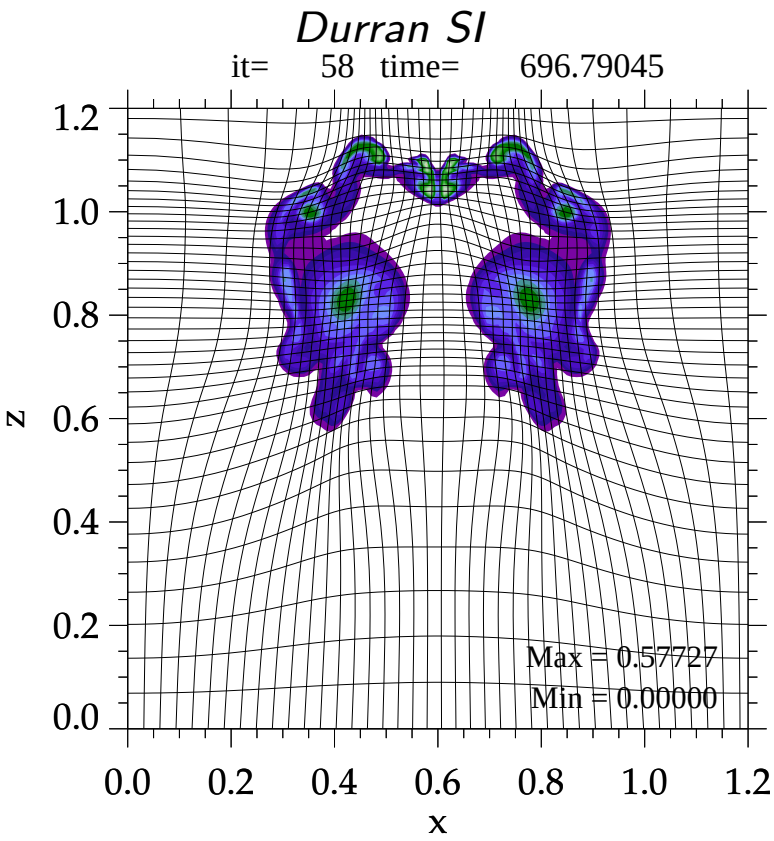

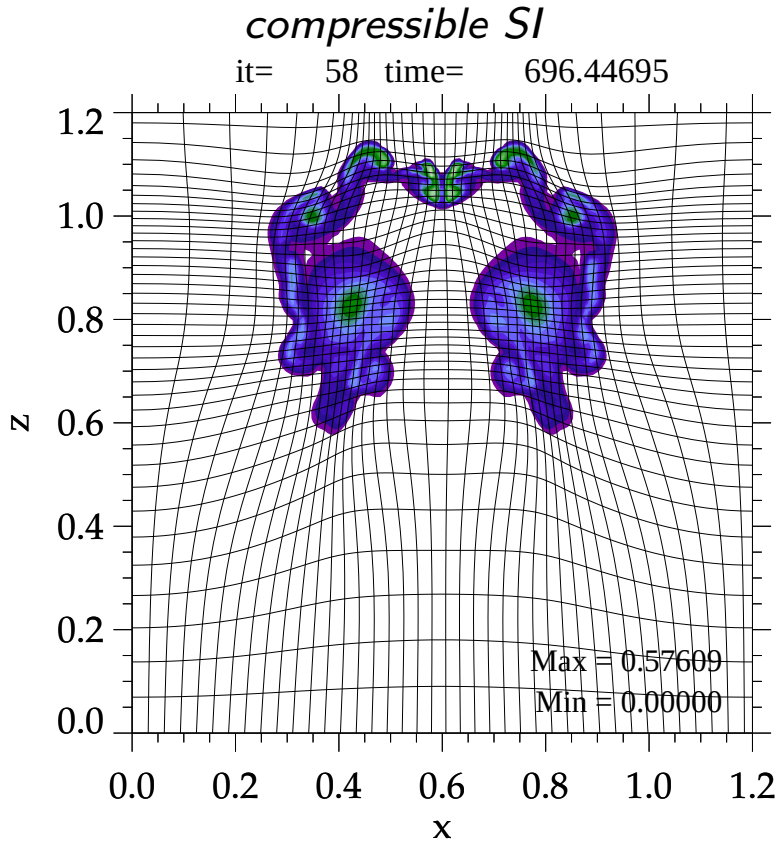

$\rightarrow$ mesh refinement indicator: $\Phi = ||\nabla\theta||$

Baroclinic wave life cycle experiments with adaptive moving meshes

- → zonally-periodic channel 10000 km × 8000 km × 18 km
- → baroclinically unstable jet flow (Bush and Peltier, JAS 1994)
- → perturb initial state by local θ-anomaly at tropopause
- → integrate for 12 days

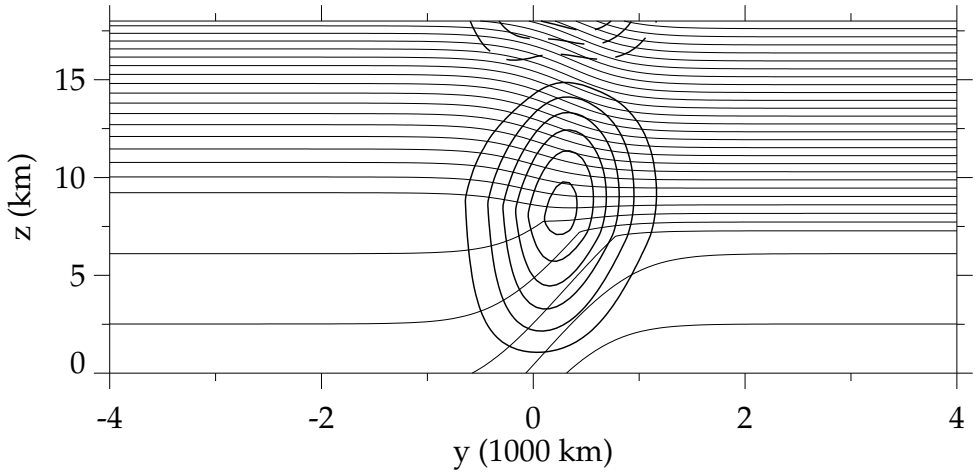

- → Coordinate mapping:

$$(\overline{x}, \overline{y}, \overline{z}) = (E(t,x,y), D(t,x,y), C(t,x,y,z)) : \quad \mathcal{D}_p \to \mathcal{D}_t$$

Baroclinic wave life cycle experiments with adaptive moving meshes

- → zonally-periodic channel 10000 km × 8000 km × 18 km
- → baroclinically unstable jet flow (Bush and Peltier, JAS 1994)
- → perturb initial state by local θ-anomaly at tropopause
- → integrate for 12 days

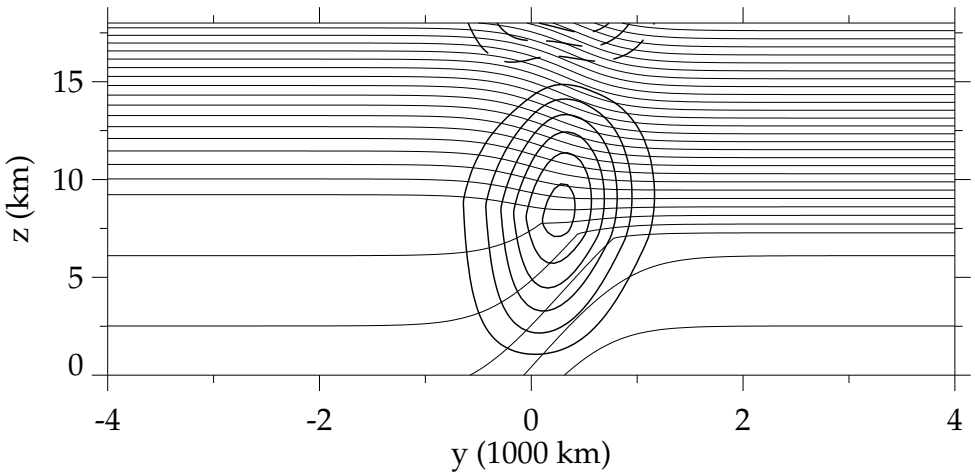

- → Coordinate mapping:

$$(\overline{x}, \overline{y}, \overline{z}) = (E(t,x,y), D(t,x,y), C(t,x,y,z)) : \quad \mathcal{D}_p \to \mathcal{D}_t$$

Baroclinic wave life cycle experiments with adaptive moving meshes

(Kühnlein et al. JCP 2012)

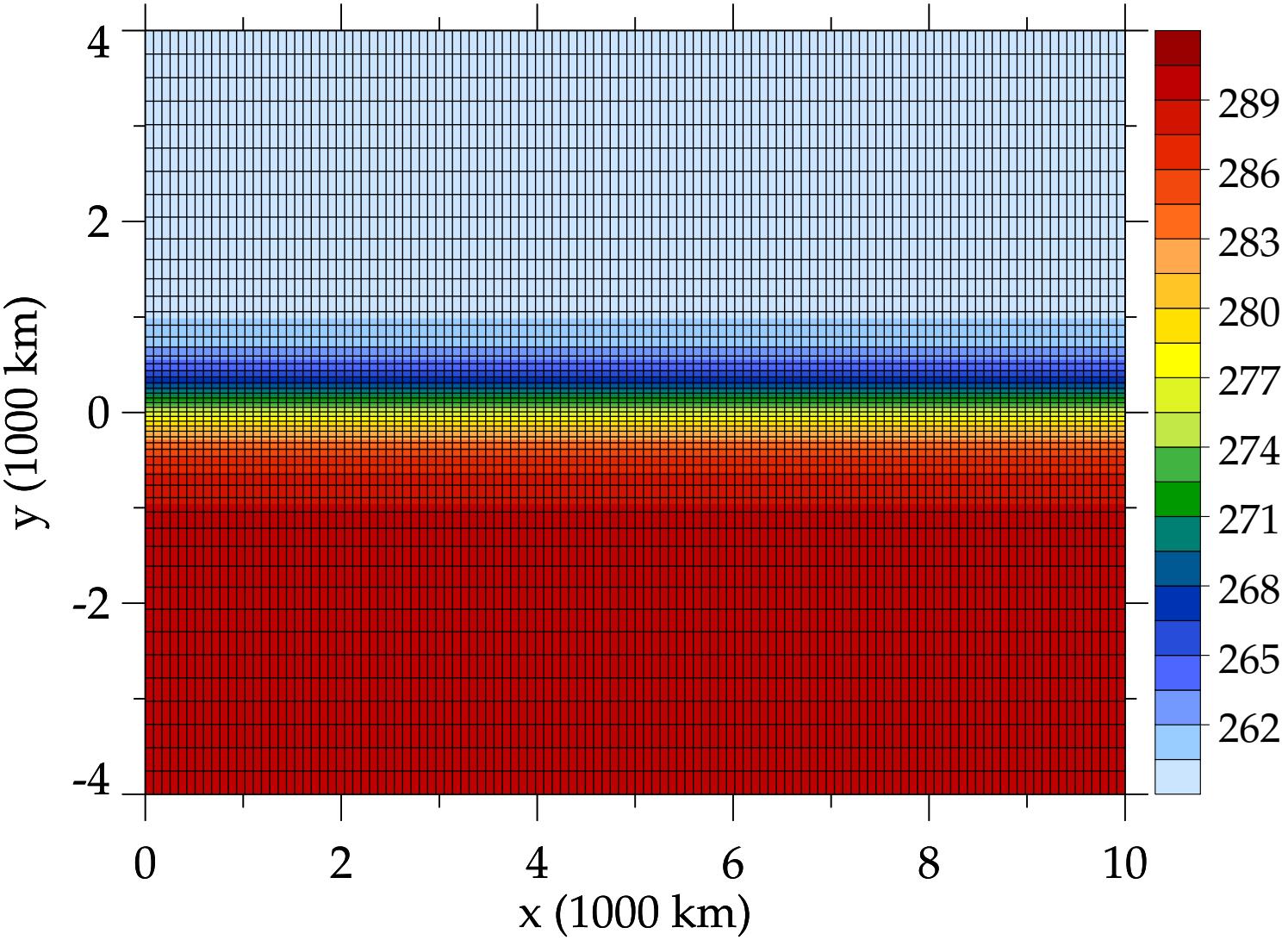

$\rightarrow$ mesh refinement indicator: $\Phi = ||\nabla_h \theta(z = 600\,\mathrm{m})||$

Baroclinic wave life cycle experiments with adaptive moving meshes

S7050

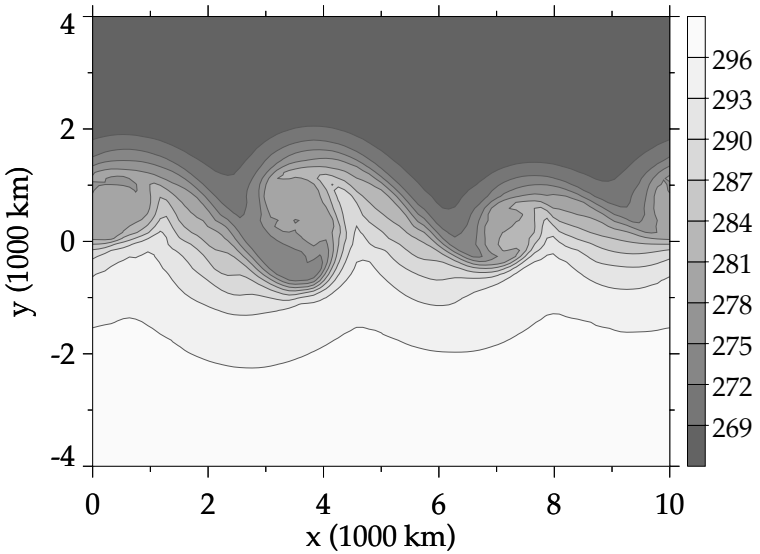

S15429

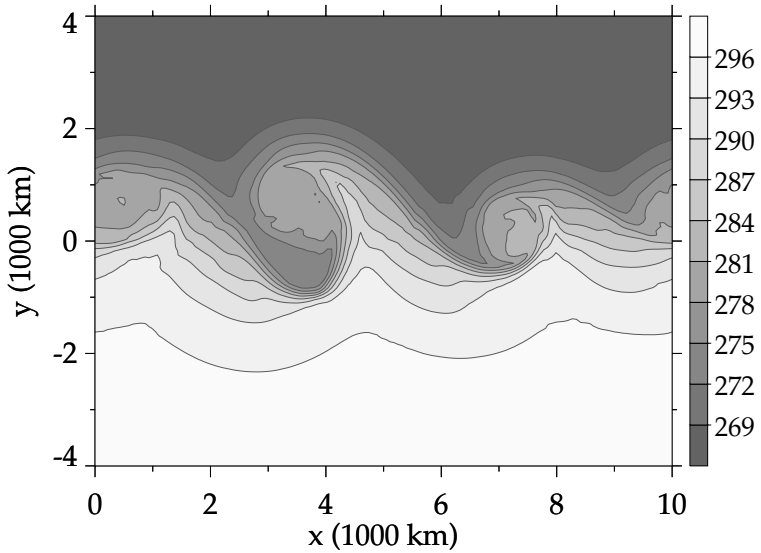

S62217

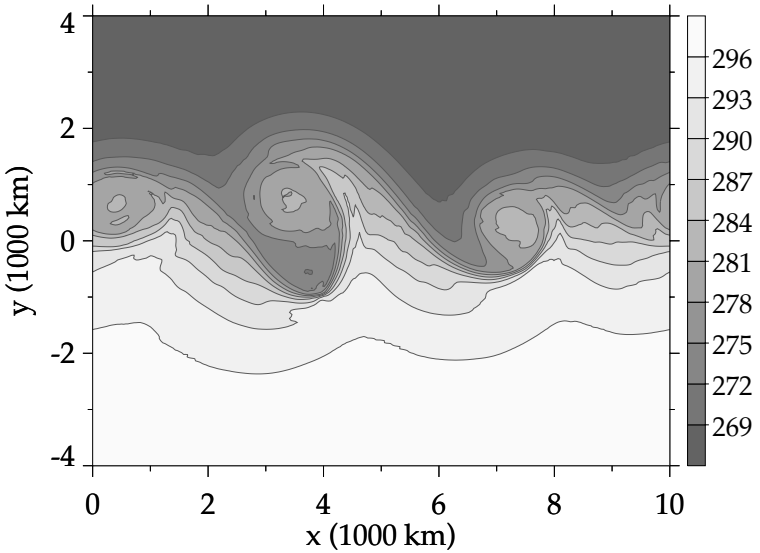

A6254

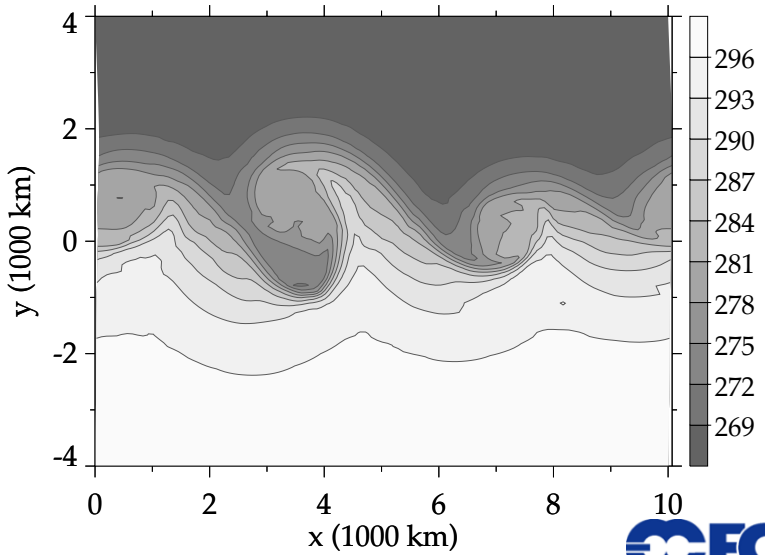

temperature field at $z = 2$ km and $t = 234$ h

Domain-averaged kinetic energetics with integration time

total kinetic energy $\langle \mathrm{KE} \rangle$

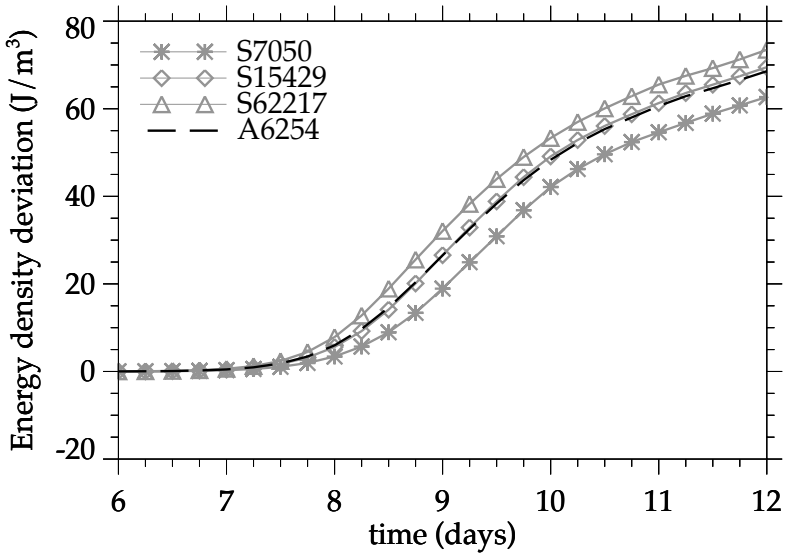

eddy kinetic energy $\langle \mathrm{EKE} \rangle$

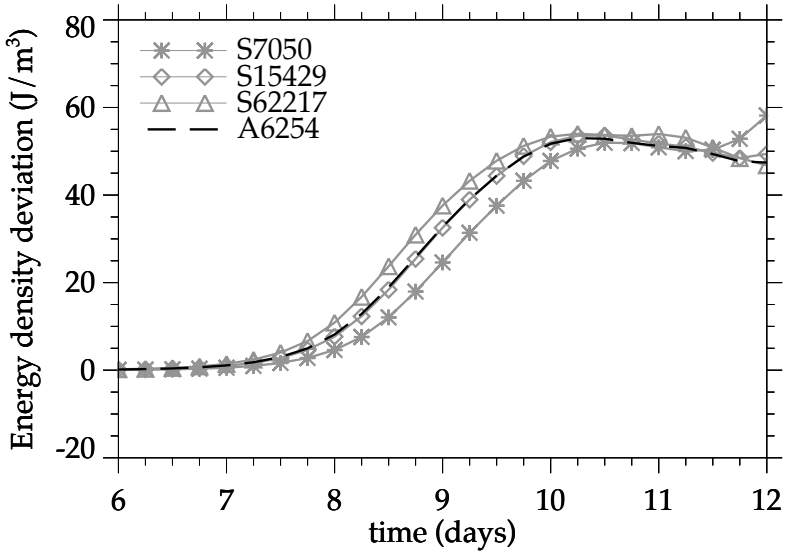

zonal kinetic energy $\langle \mathrm{ZKE} \rangle$

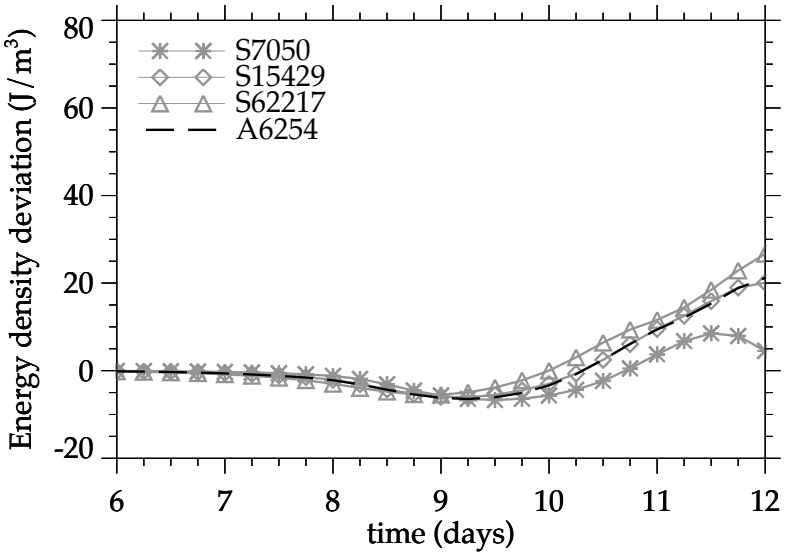

Sensitivity to mesh refinement indicator

Simulation	Refinement indicator $\Phi(t, x, y)$	$\mathcal{E}_{\langle \mathrm{KE} \rangle}$	$\mathcal{E}_{\langle \mathrm{ZKE} \rangle}$	$\mathcal{E}_{\langle \mathrm{EKE} \rangle}$
S7050	-	6.43	4.99	4.84
S15429	-	2.58	1.66	1.90
A6254a	$\frac{1}{H}\int_0^H \lVert\nabla_h\theta\rVert\, dz$	2.82	1.67	1.80
A6254b	$\lVert\nabla_h\theta(z=600\text{ m})\rVert$	3.75	2.64	2.28
A6254c	$\lVert\nabla_h\theta(z=3000\text{ m})\rVert$	2.91	1.57	1.92
A6254d	$\lVert\nabla_h\theta(z=5100\text{ m})\rVert$	2.98	2.43	1.98
A6254e	$\frac{1}{H}\int_0^H \lVert\nabla \times \mathbf{v}\rVert\, dz$	2.90	2.10	1.83
A6254f	$\frac{1}{H}\int_0^H \lvert PV\rvert\, dz$	3.81	2.31	2.45
A6254g	$\lvert PV(z=5100\text{ m})\rvert$	4.65	2.48	2.97
A6254h	$\lvert PV(z=9000\text{ m})\rvert$	4.22	2.62	2.64
A6254i	$\frac{1}{H}\int_0^H \lVert\nabla_h PV\rVert\, dz$	3.82	2.36	2.65
A6254j	$\frac{1}{H}\int_0^H \lvert PV\rvert\, dz$, $\frac{1}{H}\int_0^H \lVert\nabla_h PV\rVert\, dz$	3.84	2.27	2.52
A6254k	$\frac{1}{H}\int_0^H \lvert EPV\rvert\, dz$	10.77	5.43	8.57
A6254l	$\lvert EPV(z=5100\text{ m})\rvert$	9.50	4.60	7.56

$$\mathcal{E}_\vartheta = \left(\frac{1}{N_o} \sum_{i=1}^{N_o} \left(\vartheta_i - \vartheta_i^R \right)^2 \right)^{1/2} \qquad \forall \quad \vartheta = \langle \mathrm{KE} \rangle \, , \langle \mathrm{ZKE} \rangle \, , \langle \mathrm{EKE} \rangle$$

$\rightarrow$ ϑ^R is high-resolution reference simulation S62217 with static uniform mesh
$\rightarrow$ $N_o = 48$ is number of 6-hourly model outputs over integration period of 12 days

Multiscale performance

→ Representation of internal gravity waves occurring in response to imbalances in the evolving baroclinic wave flow:

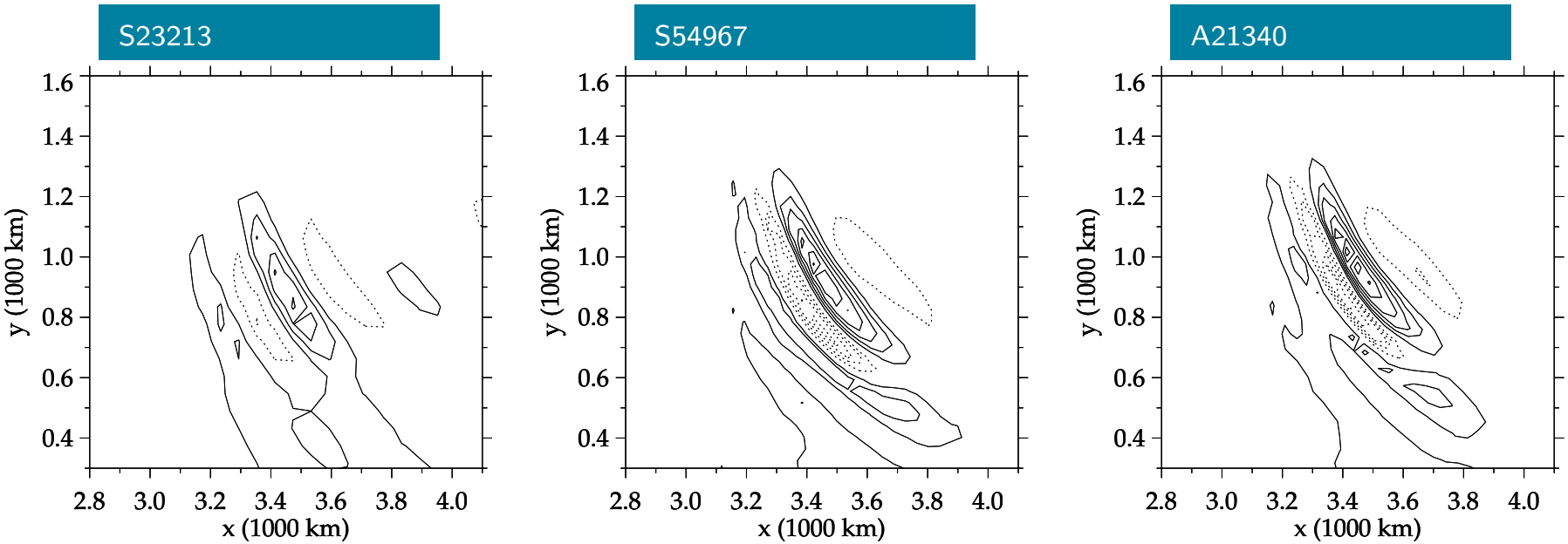

vertical velocity field at $z = 12$ km and $t = 246$ h

Adaptive moving meshes on the sphere

→ Mesh generation using optimal transport (Weller et al. JCP 2016):

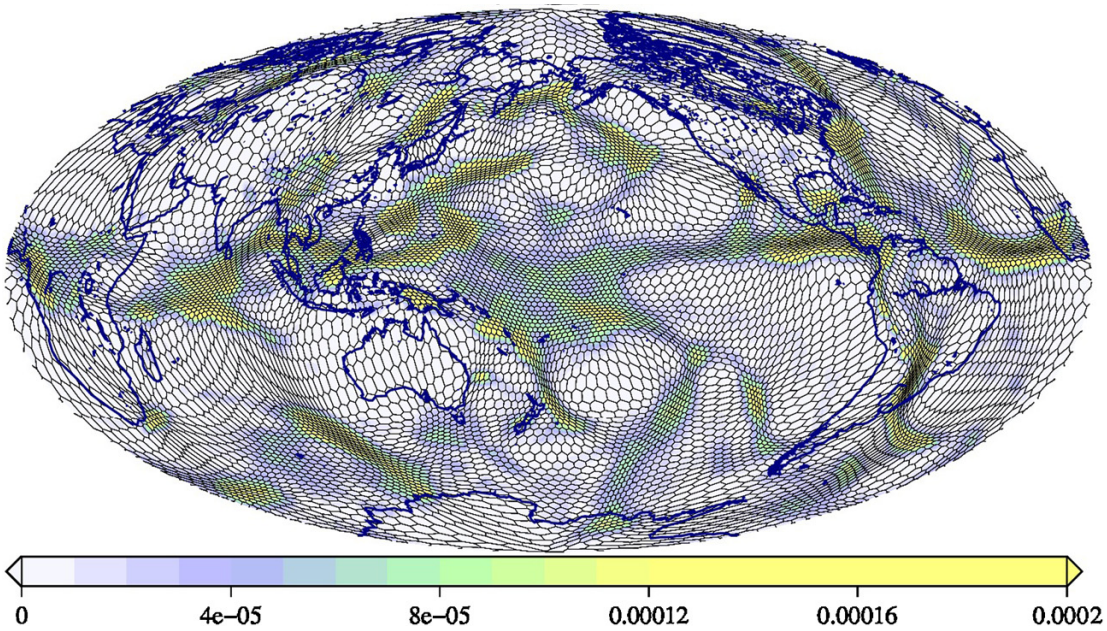

Adaptive moving meshes

Adaptive moving meshes:

+ efficient way of employing mesh adaptivity
+ keeps grid/data structure
- less flexible than h- or hr-adaptive techniques

→ Mesh refinement criteria ?

→ Subgrid-scale parameterisations ?

→ ...

- Behrens, "Adaptive atmospheric modeling", Springer 2006
- Weller et al. BAMS 2010

⇒ Workshop on moving and adaptive meshes for global atmospheric modelling, 3-5 Sep 2018, University of Reading